THEORETICAL STUDIES OF THE RS CANNUM VENATICORUM STARS

Grant NAGW-5

NATIONAL AERONAUTICS AND SPACE ADMINISTRATION

Annual Report

Period: January 1, 1980 - December 31, 1980

Principal Investigator: Dermott J. Mullan

Bartol Research Foundation of The Franklin Institute
University of Delaware, Newark, Delaware 19711

Submitted: March 4, 1981

In the proposal, four areas of research interest were singled out for attention: (i) Chromospheric modelling; (ii) Starspot modelling; (iii) STL crossing (where STL denotes "supersonic transition locus"); and (iv) STL crossing and T Tauri phenomena. When the proposal was originally submitted, it was not obvious that we would necessarily find a close physical relationship between the results in any two of these four areas of research. As it turns out, however, in the course of the research which we have carried out during the first year of the Grant period, our results are now hinting at an interesting convergence between three of the four areas, viz. (i), (iii), and (iv). In order to highlight how this convergence has come about, and how a more unified, global view of RS CVn atmospheres has emerged in terms of magnetic stability arguments, it is convenient to rearrange the ordering in this report, and describe the progress in the following order: (iii), (i), (iv), and (ii).

First Topic: (iii) STL crossing

(a) Introduction

The etymology of the term STL is relevant in the present context. The term was coined by Mullan (1978) in order to characterize the state of the atmospheres in certain late-type giants. In giant stars, the process of mass loss by means of a stellar wind is facilitated (relative to the solar case) by the low gravity. As a result, if the wind is thermally driven (as Parker originally suggested for the solar wind), then even a rather small coronal pressure suffices to accelerate the wind rapidly to the sound speed. Hence, in general, the sonic point is expected to lie closer to the stellar surface than in the solar case (other things being equal).

Mullan (1978) was interested in the physical processes which would occur as the sonic point approached closer and closer to the stellar surface. He devised a semi-empirical technique to estimate the radial distance of the sonic point: the technique combined empirical estimates of coronal gas pressures with a theoretical modelling scheme for stellar coronae. This technique, when combined with stellar evolutionary tracks, allowed Mullan to derive a locus in the HR diagram along which the sonic point sinks very close to the stellar surface. When this occurs, the entire corona becomes supersonically expanding. Hence, along this locus, stellar coronae would be expected to make a fundamental transition to a completely supersonic state. Hence the name: supersonic transition locus. Mullan suggested that STL crossing might be physically related to three processes: (1) increased rate of mass loss; (2) penetration of detectable mass loss flows into deeper layers of the atmosphere; (3) opening up of magnetic field lines in the stellar corona. The only data available to Mullan at the time that work as done (1977) were circumstellar absorption data: these did indeed show that onset of circumstellar absorption occurs in the HR diagram along a boundary close to where Mullan derived the STL. This was considered as evidence in support of process (1).

(b) More recent developments

Evidence in favor of process (2) has been obtained recently by Stencel and Mullan (1980), who examined the asymmetries of emission cores of Ca and Mg resonance lines in a large sample of late-type stars. When mass loss becomes rapid, the central absorption component is shifted to the blue, resulting in a weakening of the shortward (S) component relative to the longward (L) component. Hence, the intensity ratio S/L serves as an indicator of rapid mass loss when S/L falls below unity. Stencel and Mullan examined samples of stars to determine where in the HR diagram S/L < 1 occurs for Mg and Ca. It is important to recognize that the Mg emission is formed at higher atmospheric levels than the Ca emission. Results for the boundaries along which S/L < 1 occurs are shown in Fig. 1: these are significant in the light of evolutionary considerations. For evolved stars in the part of the HR diagram shown in Fig. 1, evolution carries the stars from left to right. Hence, they cross the mass-loss boundary in Mg before they cross the boundary in Ca. This suggests that indeed, the mass loss penetrates down to the deeper layers where Ca lines are formed at a later time than when the mass loss makes its presence felt at the level of Mg formation, higher up in the atmosphere.

Evidence in favor of process (c) has emerged from Einstein satellite X-ray data (Ayres et al, 1980). There is no detectable X-ray emission from giants and supergiants lying redward of the boundary labelled (X-rays) in Fig. 1. In the solar atmosphere, closed loops of magnetic flux are the most prolific emitters of X-rays. This is presumably true in other stars also. Hence, the Einstein data are consistent with Mullan's (1978) suggestion that closed magnetic field lines cannot exist above the STL. Further evidence that there is little or no hot material in the atmospheres of stars in the cool giant part of the HR diagram was derived from the IUE data by Linsky and Haisch (1979). Their dividing line, between hot and cool coronae is shown in Fig. 1 also.

The most remarkable aspect of the dividing lines in Fig. 1 is that they lie so close to one another as to be essentially identical. This is important because it shows that rapid mass loss sets in precisely among those stars where hot material is lacking. Hence, there is essentially no thermal pressure to drive a stellar wind. This is the first piece of evidence to suggest that the mass loss process in cool giants may be different from the canonical thermal wind picture which has been the accepted model for the solar wind for 20 years.

(c) Importance of the RS CVn stars

It happens that Stencel and Mullan's sample of stars included 10 subgiants. Results for the S/L asymmetry ratio for these stars are shown in Fig. 2. The onset of rapid mass loss (i.e. S/L < 1) occurs among subgiants of early K spectral type. This is significant

in view of the fact that the active stars in many RS CVn systems are also subgiants of early K spectral type (Popper, 1970) (see Fig. 2). This leads us to conclude that activity and rapid mass loss may be physically related. I believe that the RS CVn systems may hold the key to what the relationship is.

(d) Inapplicability of thermal wind

As has been noted above, thermal wind interpretations of the mass loss process in late-type giants are unlikely to be valid: there seems to be no thermal pressure available, for one thing. Further evidence to support this conclusion has been given by Holzer (1980) from a theoretical point of view, and by O'Brien (1980) from an observational point of view. Holzer showed that if the sonic point sinks so low as to enter the chromosphere (as the STL concept had envisaged), then the mass loss rate would not in fact increase abruptly. At least, this is the conclusion to be drawn if the wind can be treated as spherically symmetric and steady in time. (In the event that spherical symmetry is not assumed, but spicules are allowed to be present, this conclusion of Holzer's may no longer be true: cf. Wallenhorst, 1980). As regards O'Briens's observations, these referred to line profiles of the chromospheric/coronal spectral line of neutral helium at a wavelength of 10830 Å. O'Brien obtained a number of high resolution line profiles at various epochs in various cool giant stars. In some of the giants (the warmer ones), the line profiles remain largely unchanged as a function of time. However, variability in the profile becomes very pronounced above a certain boundary in the HR diagram, and this boundary coincides well with the various boundaries in Fig. 1. Thus, the mass loss process in these stars is not steady in time, or spherically symmetric, or both. However, the standard thermal wind scenario involves both spherical symmetry and steady state.

This led me to propose a non-thermal mass loss process in giants, based on magnetic reconnection. (It so happened that I presented the model at a meeting (the Harvard Cool Star Workshop) immediately following the talk by Holzer in which he showed the inapplicability of thermal wind ideas.) The scenario for mass loss is shown in Fig. 3. At $t = 0$, a magnetic loop emerges through the stellar surface. Due to some instability (see below), the loop balloons upwards (b), and in the process, outside pressure plus internal currents cause the legs of the loop to be pinched, forming an x-type neutral point (b). Reconnection here leads to the formation of disconnected loops of field in the upper part (c), until finally at time t_{rec}, reconnection is complete, and the loop severs its connection with the stellar surface. Lorentz forces on the loop then force it upwards, and eject it from the star. Thus, mass loss occurs in the form of "blobs" of matter plus field which break away from the star at random intervals and in random places. Concepts of spherical symmetry and steady state have no place in such a model. We identify the blobs of magnetic material with the

mass-loss events recorded by O'Brien in his He I 10830 line profile data.

(e) Testing in the sun

One of the most interesting results to emerge from our research has been the possibility to test this mass loss scenario in a "local" laboratory, the sun. The solar mass loss process occurs mainly from coronal holes. This in itself represents a departure from spherical symmetry. However, an even more radical departure from spherical symmetry in the solar mass loss process has emerged recently from Skylab data (Davis, 1980): the solar wind density appears to be positively correlated with the numbers of X-ray bright points in solar coronal holes. Davis had been led to search for such a correlation from earlier work of Ahmad and Webb (1978) which suggested that indeed mass is being ejected upwards from X-ray bright points in coronal holes. The result is remarkable, for it suggests that the mass loss in coronal holes is somehow related to conditions in a few extremely localized sources.

It seems natural to apply the ideas of Fig. 3 to this problem. I have therefore been collaborating with Dr. I. A. Ahmad in this regard. The results of our collaboration suggest that the scenario in Fig. 3 is indeed consistent with a variety of solar coronal hole data. Since the scenario is a radical departure from canonical ideas about mass loss, it is worthwhile to describe here what these consistency checks are.

Since Ahmad and Webb (1978) were able to derive a mass loss rate from the X-ray bright points, we can use the mass in a bubble such as that shown in Fig. 3 (d) in order to estimate how often a bubble must be pinched off at the solar surface and ejected upwards. The results are that pinching must take some 300-1000 seconds in the sun. It is interesting that X-ray bright points have been observed to vary in intensity on time scales of precisely this order (Sheeley and Golub, 1979; Habbal and Withbroe, 1980). The reconnection time scales that this process demands therefore lead us to an estimate of the field strengths in the X-ray bright points. When we combine these with estimates of the gas pressure and lengths of the loops, we can enter the criteria established by B. C. Low (1980) for the onset of ballooning instability. We find that the field strengths in the X-ray bright points are in fact larger than critical, and that therefore the ballooning process which is postulated to occur in Fig. 3 (a)-(b) will in fact occur. We identify the energy release in the reconnection site in Fig. 3 (b) with the X-ray bright points in process of flaring. Thus, we are consistent with Davis (1980) result that X-ray bright points are somehow related to the mass loss process.

As regards the upward motion of the bubble in Fig. 3 (d), the occurence of density stratification in the corona causes the bubble to expand. We have calculated how this expansion should occur,

and we find bubble radii as shown in Fig. 4. Notice that the expansion of a bubble is very rapid in the low corona (where the density stratification is exponentially steep), and much more gradual higher up (where the density variation is slower). For comparison, we also show an empirical determination of coronal hole boundary size (Munro and Jackson, 1977). The shapes are quite similar. Hence, although the X-ray bright points occupy only a small fraction of the solar surface close to the photosphere, the bubbles breaking away from the bright points expand so much that they occupy essentially all of the coronal hole area at altitudes of a few solar radii.

Further consistency checks are obtained when we consider the ultimate fate of the bubbles. They eventually lose their identity and deposit their internal magnetic and thermal energy and momentum into the solar wind. We have been able to estimate where the dissolution process should occur. The results are quite insensitive to the various coronal parameters, and they indicate that at altitudes of order $(1-2)R_{sun}$ above the photosphere, the bubbles should dissolve. It is interesting that it is at precisely altitudes of this order where energy and momentum is apparently being fed into the coronal hole wind. (This is an empirical result: Munro and Jackson, 1977; however no theoretical explanation has previously been proposed as to why the energy deposition should occur at such altitudes.)

Finally, the rapid expansion of a bubble in the low corona (i.e. much faster than radial expansion) has the effect that the sonic point of the flow is lowered: the sonic point may lie as low as $(0.1-0.2)R_{sun}$ (Kopp and Holzer, 1976). Hence, with bubble dissolution occurring at altitudes of order $(1-2)R_{sun}$, the energy being deposited by this dissolution process is entering the wind in its supersonic regime. There is an important effect which ensues in such a case: the flow speed at infinity is raised appreciably (Leer and Holzer, 1980). Since it is in fact known that the wind emerging from coronal holes has very high speed at infinity, this is one further consistency check on the scenario.

On the basis of this work, therefore, we conclude that the mass-loss scenario presented in Fig. 3, in which mass-loss is driven by magnetic reconnection, is consistent with all of the major properties of coronal hole mass outflow in the sun.

(f) Application to warm giant stars

In order to apply the scenario in Fig. 3 to giant stars, it is first of all necessary to ask why a magnetic flux loop should balloon upwards in such a star? We do not have access to the detailed information which was available to us in the case of solar X-ray bright points, so we cannot rely on the type of ballooning instability which we relied upon to understand why ballooning should occur in the sun. However, we have identified a much more

general criterion for onset of magnetic instability among the giant stars, as follows.

Pneuman (1968) has considered the equilibrium flow pattern around a closed loop of magnetic flux in the solar corona. On the closed loop, and beneath it, outflow is impeded because of the high electrical conductivity of the coronal gas. Hence, in this region, the gas can be considered to be in magnetohydrostatic equilibrium. The closed field lines extend up to a radial distance R_{cf}. Above this, and also around the sides of the loop closer to the solar surface, mass can flow outward freely along open field lines, driven by thermal pressure. (The combination of closed field lines low down and open flow higher up gives rise to a feature resembling what coronal observers have long labelled as a "helmet streamer".) Pneuman shows that the thermally driven flow passes through a sonic point at a radius R_{sp} which is not greatly different from the result derived by Parker for the strictly spherically symmetric case, i.e. $R_{sp} \simeq (4\text{-}5) R_{sun}$. For our present purposes, the result which is of greatest significance in Pneuman's work concerns the relationship between R_{sp} and R_{cf}. Pneuman finds $R_{sp} = 2\ R_{cf}$. Thus, he predicts that closed field lines in the solar corona extend no further than to altitudes of 1-1.5 R_{sun} (i.e. to radial distances of 2-2.5 R_{sun}). This is consistent with eclipse data: the best exposed photographs rarely if ever show closed loops extending beyond such radial distances.

Consider, now, the case of a star where, if there were to be a thermally driven wind blowing, R_{sp} would happen to be $\lesssim 2\ R_{star}$. What will happen when a new loop of magnetic flux emerges from beneath the surface of such a star? If the loop were to be in equilibrium, then the closed part of the loop structure would be confined to radial distances less than $R_{cf} = 0.5\ R_{sp} \lesssim R_{star}$, i.e. <u>inside</u> the star. Closed loops <u>outside</u> the stellar photosphere can find no equilibrium in such a case. Hence when a closed loop of flux emerges into the corona, the loop is always unstable, and must enter a phase of dynamical evolution immediately upon entering the corona. The initial phase of dynamical evolution is expected (Low, 1980) to be in the form of ballooning. This therefore sets the stage for the scenario in Fig. 3 to begin.

(g) A new transition locus in the HR diagram: the magnetic topology transition locus (MTTL)

Previously, the STL had been defined in terms of the sonic point lying <u>at</u> the stellar surface: $R_{sp} = R_{star}$ (Mullan, 1978). In view of the above discussion, this is certainly a sufficient condition to ensure that magnetic flux loops in the atmosphere will be unstable. However, it is not a necessary condition for loop instability. The onset of instability requires only that $R_{sp} = 2\ R_{star}$. This suggests that we should derive the locus in the HR diagram along which $R_{sp} = 2\ R_{star}$, using the same technique as before for the STL. Below this new transition locus, magnetic

loops can remain closed for long periods of time in the stellar corona, as in the sun, for example. However, above the locus closed loops cannot be static features. Instead they must be regarded as in a perpetual state of evolution towards another form, presumably eventually open. Thus, the transition is essentially the type of magnetic transition outlined in Mullan (1978): viz. from closed to open topology. For that reason, we refer to the new transition locus as a magnetic topology transition locus (MTTL).

To find the MTTL, we have used three of the evolutionary tracks computed by Paczynski (1970). Results are shown as circled x's in Fig. 5. Also shown in Fig. 5 are the individual stars in the sample of Stencel and Mullan (1980), differentiated according to their S/L ratio being less than unity (rapid mass loss) or greater than unity. These are the data from which Stencel and Mullan deduced the "velocity dividing line" (labelled VDL in Fig. 5) separating rapid mass loss stars from those without rapid mass loss. (The temperature dividing line (TDL) derived by Linsky and Haisch (1979) is also shown in the figure.) The important conclusion from Fig. 5 is that the MTTL and VDL coincide rather well. Thus we are led to believe that the onset of rapid mass loss is closely correlated with the onset of dynamical magnetic field behavior in stellar coronae. It is also interesting that the presence of hot material in stellar coronae seems to disappear at precisely the region where closed magnetic flux loops can no longer exist in static equilibrium in the corona.

This leads us to conclude that dynamic magnetic field behavior contributes to rapid mass loss in warm giant stars. Since these stars have no appreciable thermal pressure to drive a steady, spherically symetric wind of the kind discussed by Parker for the solar wind, we propose that the properties of dynamic magnetic fields are such that they can drive mass loss efficiently. In particular, we propose that the scenario in Fig. 3 may be at work in warm giant atmospheres as a form of magnetically driven mass loss. Hence, we envision the atmospheres of these stars to be in a state of continual magnetic upheaval. This is in great contrast to the solar corona, where closed loops of magnetic material can exist in relatively static equilibrium for days on end.

The MTTL concept avoids the most serious objection to the STL concept, as raised by Holzer (i.e. the difficulty with the sonic point entering the chromosphere): in the present case, the sonic point remains far out in the corona, and there is no question of the sonic point entering cool chromospheric material.

The viability of our proposed magnetically driven mass loss scenario depends on the existence of magnetic fields (particularly in the form of newly emerging closed loops of flux) in warm giant stars. It must be admitted that direct evidence for such fields is essentially non-existent. However, it seems quite plausible that warm giants will possess surface magnetic fields because of the presence of deep convection zones near their surfaces. In fact, Wilson (1973) referred to this possibility in his interpre-

tation of enhanced calcium emission among giant stars. However, it is also useful to refer to a group of stars where we know (on the basis of independent evidence) that there are magnetic fields present. This is where the RS CVn systems prove useful.

(h) RS CVn systems

Activity in RS CVn systems is well established: there are flares in X-ray, radio, and in UV and optical emission lines. The magnetic nature of this activity is strongly suggested by the presence of intense circular polarization in the radio bursts, as well as by the photometric evidence for starspots. Hence it seems very likely that the early K subgiant star is the site of vigorous magnetic processes.

It is significant that the level of X-ray emission does not fall to zero outside flares. Large emission measures remain present even in the non-flaring state (Walter et al, 1978), and these require that mass loss in the form of hot gas must be going on from one or other star at the present time at a rate of order a few times 10^{-9} $M_\odot$/yr (Walter et al, 1978). (Note that there is a numerical error in the estimate of Walter et al: when one inserts their quoted densities and temperatures, one finds the above mass loss rate.) However, on the basis of evolutionary considerations (Popper and Ulrich, 1977), the rate of mass loss averaged over the lifetime of the stars (i.e. some 10^9 years) must be much smaller than the current rate, viz. a few times 10^{-11} $M_\odot$/yr. (We note that the evolutionary lifetimes of 10^9 years are confirmed by the occurrence of synchronization between axial and orbital angular velocity in many RS CVn systems having periods of 20 days or less (Hall, 1978): according to the formulae of Zahn (1977), this requires that the ages be 10^9 years or more.) It appears, therefore, that rapid mass loss is a <u>recent</u> occurrence of the star's evolution, occupying no more than a few percent of the lifetime. This is consistent with Stencel and Mullan's (1980) finding that early K subgiants lie close to the locus of rapid mass loss onset.

We therefore propose that crossing the MTTL has two major effects on a stellar atmosphere: it causes vigorous magnetic upheaval in the atmosphere, and it causes rapid mass loss to set in. The RS CVn systems happen to possess magnetic fields which are so large that the magnetic upheaval has other consequences (other than mass loss) which render the fields "visible" (in effect) at the Earth, i.e. magnetic activity. On the other hand, warm giants which lose mass by the magnetic scenario shown in Fig. 3, but where the magnetic fields are weaker than in the RS CVn systems, may be undergoing magnetic activity at a level which is so low as to be undetectable at Earth. Thus, Gibson (1977) searched for radio emission from early K subgiants outside RS CVn systems, and could detect no radio emission greater than 1% of the median luminosity of emission from RS CVn systems. If the emission is due to syncrotron processes, this factor of 100 (at least) suggests that the field strengths in the non-emitting stars are smaller by a factor of (at least) 3 than in the RS CVn stars. It may be that the non-RS CVn stars are single stars, and are slowly rotating because they have no orbital angular momentum to draw upon, as the closely separated RS CVn stars do.

The slow rotation can have a serious effect on the efficiency of dynamo activity: the mean field strength generated by dynamo action may scale as $|B| \sim \Omega^{\alpha}$, where $\alpha = 1\text{-}1.5$ (Kippenhahn, 1973). Thus, the field strength may be rather sensitive to angular velocity. In fact, the field strength may be even more sensitive than this power-law behavior suggests: it may involve threshold behavior (Levy and Rose, 1975).

(j) RS CVn atmospheric structure

Our view of RS CVn active secondary star atmospheres now is one in which there are no analogs to the static long-lived closed magnetic loops which are so familiar to us since the Skylab mission revealed their dominant role in the solar corona: essentially, these static long-lived loops are the solar corona. An RS CVn star has no such features. Instead, a newly emerging flux loop follows dynamical evolution, perhaps of the kind shown in Fig. 3. We have estimated the time scale to evolve from Fig. 3 (a) to 3 (d): the reconnection time t_{rec} in RS CVn systems turns out to be in the range 6-60 hours. During these times, the flux loops balloon upwards into extremely distended shapes. In fact, there are some empirical data which suggest the the X-ray emitting volumes in RS CVn systems are loops of such a kind (Swank and White, 1980), and distended loops also play an essential role in the flare scenario proposed for UX Ari by Simon et al (1980). The conclusion of our work is that such loops are not stable: they are only fleeting features in the atmosphere, living no more than 6-60 hours. It is interesting that the only estimate of time-scales for alterations in the Mg emission lines in these stars (Weiler, 1978) lies within this range, i.e. 12 hours. This leads us to propose that the prominent individual emitting features detected by Weiler (1978) in his study of Mg h and k emission variability can be identified with the dynamically unstable loops which we have discussed in connection with MTTL crossing.

If this identification is correct, then the fact that the features show up as prominent features in the line profile (rather than simply as very small, subtle features) argues in favor of the hypothesis that the emitting elements are not small compared with the stellar radius. In other words, they must be considered as macroscopically large as far as optical emission is concerned. This will be important below when we interpret observed line profiles in terms of chromospheric modelling.

Second Topic: (I) Chromospheric Modelling

(a) Isothermal models

We have constructed a grid of chromospheric models in order to compare with observed Balmer line profiles in RS CVn systems.

We begin with a photospheric model which has been computed by the standard methods of radiative/convective equilibrium. Tables of such models have been computed by (e.g.) Gingerich and Rich (1969) (GR), by Bell and Gustaffson (1980), among others. These models extend upwards to typically continuum optical depths of order 10^{-3}. Our models of "isothermal chromospheres" consist of the photospheric model up to this highest level, plus an extension at even higher levels where the temperature is forced to remain constant, and equal to the last temperature in the published photospheric model. With that choice of temperature structure, we compute the Balmer line profiles as follows.

In the given temperature structure, the equation of hydrostatic equilibrium is solved for the density structure, and the first iteration for populations of various levels and various stages of ionization. With these inital guesses for the populations, the non-LTE radiative transfer problem for a hydrogen atom containing five bound levels plus a continuum is solved by the method described in Cram and Mullan (1979). The transfer equation is solved explicitly for the transitions Hα, Hβ, and Hγ, and also for the Lynam, Balmer, and Pascehn continua. Fixed rates are assigned to the remaining (two) continua and (three) lines. When the radiative transfer has converged the first time, the new level populations are iterated again through the equation of hydrostatic equilibrium. The reason that this new iteration is required is that we are solving the radiative transfer problem for the major constituent of the atmosphere (hydrogen), so that changes in level populations and ionization equilibria due to the radiation field can be sufficiently large to force the atmosphere out of hydrostatic equilibrium. Hence, several iterations and re-iterations through both hydrostatic equilibrium as well as radiative transfer convergences are required to obtain overall convergence. Typically five iterations of each cycle are called for in order to reduce the changes between succeeding iterations to less than 1% for all transitions. In solving the radiation transfer problem, the lines are included somewhat crudely, with only 17 frequency points per line, extending out to some 15 Doppler widths from line center. This is sufficiently accurate for the transfer problem, but in order to compute line profiles, the converged model is read in to a second routine for calculating flux profiles more precisely. This routine includes 10 angles and 75 frequency points from -20 A to +20 A from line center.

The most complete grid of photospheric models ar present seems to be that of GR and we have used that to compute our grid of isothermal model chromospheres. At the time of writing, our grid consists of models with T_e = 4000, 5000, and 6000K, and log g = 2, 3, and 4. These span most of the region on the HR diagram which are of interest in RS CVn studies. Profiles of Hα for these models are shown in Fig. 6. Notice that the effective temperature is the dominant variable, as regards both the central depth of the line and also the existence of extensive wings in the line. Clearly, our temperature grid is too coarse at present and must be filled in by intermediate T_e values.

For comparison, we have also used two models from the grid of Bell and Gustaffson (1980), viz. T_e = 5000, log g = 3.0, and T_e = 4500, log g = 3.75. Results for the first of these are shown in Fig. 7 (in which we have imposed an isothermal chromosphere). When we compare Fig. 7 with Fig. 6 (e), we find no detectable difference between the Hα profiles. The Bell-Gustaffson models incorporate a treatment of line blanketing into the modelling scheme which is considerably more sophisticated than that used by GR, and yet it seems that this makes no essential difference as far as the Hα profile is concerned. Hence, although in our discussion below, we refer to the models of GR, we expect that no essential differences would have occurred if we had used the models of Bell and Gustaffson.

(b) Non-isothermal chromospheres

The essence of semi-empirical chromospheric modelling consists in imposing a more realistic temperature structure than simply an isothermal extension of the photospheric model. In Fig. 8, we show the temperature structures which we have imposed on a particular photospheric model (T_e = 5000, log g = 3.0; this is the model which agrees most closely in our grid with the conditions in the RS CVn star λ Andromedae: for this star, $T_e \approx 4800$ K, log g ≈ 3.1. See below.). The temperature is forced to increase linearly with decreasing log m (where m is the mass loading) up to T = 8000 K. At that point (where $m = m_o$), hydrogen ionization becomes so rapid that we allow the temperature to rise essentially instantaneously to corona values. Hence for a given photosphere, our chromospheric models are characterized by essentially a single parameter, m_o. (We have also experimented with a three-segment model chromosphere, in which there are linear increases of t with log m with different slopes in the "low chromosphere" (T < 5500 K) and in the "upper chromosphere" (5500 < T < 9000 K), followed then by an abrupt jump to coronal temperatures. However, only one model of this kind has been computed so far, and we will not discuss it further here.

For illustrative purposes, we restrict our discussion to one photospheric model, T_e = 5000 K, log g = 3.0, for which we have computed three chromospheric models. The temperature structures for these three are shown in Fig. 8, where we have used log m_o = 5.25, -4.75, and -4.0. For comparison, an empirically derived model for a feature in the solar atmosphere (Vernazza et al, 1980; their model C) is also shown. The simplification associated with linear segments of T versus log m is apparent from this type of comparison. However, the current state of the art as far as stellar line profile information is concerned is such that we would not be justified in going to more refined temperature structures in our modelling attempts at present. Note that the RS CVn model chromospheres start at mass loadings, which are similar to, and slightly greater than, the solar case.

The results from one of the converged models are shown in Fig. 9, where we show the altitude variation of proton number

density and total hydrogen nucleon number density. The broad plateau in proton number density is not atypical of our models. Solar models show a similar feature.

Results for the Hα profiles predicted by the three chromospheric models are shown in Fig. 10. Notice that the predominant characteristic remains: Hα is an absorption line in such atmospheres, despite the presence of a chromosphere which starts deeper than the solar chromosphere (deeper, i.e. in terms of mass loading: cf. Fig. 8) It is in fact well known (Bopp and Talcott, 1978) that most RS CVn systems outside flares show Hα in absorption. The important conclusion to emerge from Fig. 10 is that this empirical result cannot be construed as evidence for the absence of a chromosphere.

In Table 1 we list the equivalent widths (EW) and full-widths at half-maximum (FWHM) (in parentheses) for the three lines in our models. (Negative values of equivalent width denote absorption.)

TABLE 1. Widths of Balmer lines in model chromospheres: EW (FWHM) in Angstroms

Model	Isothermal	$\log m_o = -5.25$	$\log m_o = -4.75$	$\log m_o = -4.$
Hα	-0.89 (0.72)	-1.17 (0.88)	-1.15 (0.88)	-0.99 (0.84
Hβ	-0.94 (0.51)	-1.16 (0.60)	-1.14 (0.60)	-1.01 (0.44
Hγ	-0.93 (0.49)	-1.11 (0.58)	-1.08 (0.62)	-0.95 (0.78

We notice that the Balmer decrements are very shallow, or even slightly inverted in the deepest chromosphere. We also note that for any particular line, the EW is not very sensitive to the depth of the chromosphere (i.e. to m_o: this is what we refer to as the "depth of the chromosphere": more precisely it is the depth at which hydrogen ionization sets in.) This is partly explained by the fact that a large contribution to the EW comes from the broad wings, and these are mostly photospheric in origin. The FWHM is a somewhat more sensitive indicator of chromospheric depth, at least in the case of Hγ. However, the dependence of FWHM on chromospheric depth is not monotonic: at first, the line deepens and broadens as the chromosphere is pushed to greater depths, but subsequently, the line begins to fill in with emission, and the FWHM of the absorption core decreases as a result.

The fact that RS CVn stars show Hα going into emission during large flares (Bopp and Talcott, 1978) suggests that the chromosphere is forced downwards to very low levels temporarily. This may arise from strong downward heat conduction from hot coronal plasma in the flare region.

The existence of broad wings in Fig. 10 is noteworthy from an empirical point of view. In these stars, the wings may mas-

querade as a local quasi-continuum when an observer attempts to draw in his estimated position for the true continuum in the vicinty of, say, Hα. This would result in a serious underestimate in the equivalent width from the empirical data. Hence, when we attempt to fit the observed profiles, we should not be concerned too much if the EW cannot be made to agree with observed estimates: it is more important to fit the entire line profiles in the vicinity of line center, say within ± 2 Å of line center.

(c) Comparisons with observations

Drs. B. W. Bopp and S. Smith (University of Toldeo) have generously supplied high resolution line profiles of the Hα line in 18 RS CVn systems, some systems at more than one epoch. They have also supplied us with high resolution line profiles of the calcium K emission features in these stars. A great variety of line shapes is present in their sample, from absorption to emission, from symmetric to non-symmetric, and it will be a challenge to fit all of the observed profiles.

For present purposes, we concentrate on the star λ Andromedae, for which Bopp and Smith have sent us profiles at 4 epochs. In Fig. 11, we show (half of) these profiles extending to some 2 Å from line center. These profiles have been smoothed somewhat, and they do not show that occasionally there may be some small asymmetries of red wing relative to blue wing. These asymmetries undoubtedly contain valuable information about the state of motion of the Hα-line forming regions of the atmosphere, but we have not yet had a chance to interpret them in detail in terms of systematic velocity fields. Our major interest up to the present has been an attempt to reproduce the observed great widths of the lines in Fig. 11.

The attractiveness of the star λ And is that its mass function is very small (0.0006 $M_\odot$; Baliunas and Dupree, 1980; hereafter referred to as BD). From this, we estimate that the orbital inclination is sin i $\leq$ 0.13, i.e. the system is viewed practically pole-on. Since the active star appears to have a rotational period of order 50 days, and a radius of about 6 R_{sun} (cf. BD), the rotational velocity component in the line of sight is vsin i $\leq$ 0.8 km/sec. Hence, rotational line broadening can safely be excluded when we interpret the line profiles.

We have tried to fit the four observed profiles with one or other of the four profiles which we have computed for Hα in a star with T_e = 5000 K, log g = 3.0 (i.e. we have used Fig. 6 (e) and Fig. 8). (This is difficult to do in the form that the profiles are presented here, but on transparent paper, the fitting can be attempted easily.) These attempts lead to an immediate conclusion: no fits are possible with any of our four computed line profiles. All of the latter are too narrow (and too deep) to agree with the observed profiles. At first, we had expected that simply deepening the chromosphere would fill in the central depth and broaden the line enough to fit the observed lines. But this

turned out to be impossible to do: at first, the lines did indeed widen somewhat, but never to the extent of the observed profiles. Then, emission began to fill the line in, and the full-width of the absorption feature began to decrease with deepening chromospheres. Thus, we are forced to the conclusion that the static chromospheres which we have computed cannot explain the observed broad profiles. And if we go to somewhat cooler atmospheres (after all, the temperature of λ And is somewhat cooler than our models), the problem becomes more acute.

For λ And, we cannot rely on rotational broadening. We therefore consider macroturbulent broadening. (We note that in our chromospheric modelling, we included no velocity broadening of the kind that is usually referred to as "microturbulence", although this is included in some of the semi-empirical chromospheric models which other investigators have calculated). As the simplest possible case, we consider isotropic Gaussian broadening, with a broadening function equivalent to a velocity distribution of exp $-(v/v_o)^2$ for the macroturbulent elements (Gray, 1976). In Fig. 12, we show results obtained when we apply macroturbulent broadening to the four theoretical line profiles in Fig. 6 (e) and Fig. 8. The broadening velocity parameter v_o is attached to each broadened line in Fig. 12.

Now, we compare the profiles in Fig. 12 with the empirical profiles in Fig. 11. We find the interesting result that the observed profiles can be fitted rather well. An example is shown in Fig. 13, where we show how profile No. 3 in Fig. 11 can be fitted rather well by the line from chromospheric model with log m_o = 5.25 and v_o = 30 km/sec. The fitting is good to within a few percent. We find that observed profile No. 1 can be described by means of the isothermal model with v_o = 30 km/sec with an accuracy of about $\pm$ 3% from $\Delta\lambda$ = 0 to 2 Å. Profile No. 2 can be fitted between $\Delta\lambda$ = 0.3 and 2.0 Å within $\pm$ 2% by our model with log m = -5.25 and v_o = 30 km/sec: in the line core, the theoretical line is too deep, by some 7%. Profile No. 4 can be fitted by the model with log m_o = -4.75 and v_o = 30 km/sec within $\pm$ 3% between $\Delta\lambda$ = 2.0 Å.

From these results, we conclude that the active star atmosphere in λ And contains macroturbulent elements with speeds of order 30 km/sec.

As partial support for this conclusion, it is useful to refer to BD, who obtained calcium emission line profiles with FWHM of 62-66 km/sec. Now, Lutz (1970) has shown that the FWHM is essentially identical to the velocity parameter W_o which enters into the Wilson-Bappu relationship (1957):

$$M_V = 27.59 - 14.94 \log W_o \qquad (1)$$

In BD, the value of M_V is quoted as being +1.9. They also quote

an apparent V magnitude of 3.4, and a distance of 26 parsec, from which we estimate M_V= +1.3. Inserting M_V = +1.3-1.9 into eq. (1), we find W_O = 52-58 km/sec. Hence, the observed widths are considerably greater than expected on the basis of the "normal" Wilson-Bappu relation. The difference can be interpreted in terms of an extra source of Gaussian broadening, V_m. Since Gaussian widths add quadratically (Lutz, 1970), V_m derived from the above differences lie in the range 22-41 km/sec. These are consistent with the parameter $v_o \approx 30$ km/sec which we have derived above. Moreover, BD mention that on one occasion they detected a feature in the Ca K line profile moving at some 70 km/sec relative to the star. If the macroturbulence is indeed Gaussian, with a parameter 30 km/sec, then elements moving at 70 km/sec are expected to constitute some 2% of the atmospheric velocity field. This would be consistent with BD's observation that the fast feature was detected only once, i.e. it is a rather rare occurrence.

From UV data on λ And, BD also cite evidence for turbulent broadening in the atmosphere at the level of formation of lines such as Si III and O VI (i.e. at temperatures of 10^5 K and above). Again, non-thermal velocity fields of order 30 km/sec are indicated in the atmosphere of λ And.

We note that among our sample of theoretical chromospheric models, the deepest one (with log m_o = -4.0) cannot be made to fit any of the observed line profiles of Hα. On the other hand, Baliunas et al. (1979) have computed semi-empirical models of the λ And chromosphere that are even deeper than this (with log m_o as large as -3). Although their deepest model (with log m = -3.0 and a rather hot low chromosphere) was certainly inconsistent with observed Hα line profiles (in the sense that it predicted a strong emission line, contrary to observations), yet they were able to find deep-lying models (with log m_o almost as large as -3) which yielded Hα line profiles of such a nature that they could reproduce the observed central depth and half-width within 10%. (The observations were those of Kraft et al. [1964].) Strictly speaking, our models are not comparable to those of Baliunas et al. because of the difference in T_e (they used 4600 K), and because they allowed for the existence of significant microturbulent velocities (up to sonic speeds) in their models. However, both of our results are consistent with the conclusion that it is impossible to reproduce the observed width of Hα in λ And by means of a static atmosphere: non-thermal velocities of some kind are required, either microturbulent, or macroturbulent. The fact that we have been able to use macroturbulence to reproduce some of the observed line profiles with an accuracy greater than Baliunas et al. quote suggests that macroturbulence is a more acceptable description of the atmospheric velocity field. This is particularly true since we have at hand a natural explanation for the macroturbulent velocity.

(d) The source of macroturbulent broadening

Our work above on the magnetic instability of RS CVn atmospheres suggests a natural explanation of the source of macroturbulent velocity broadening. We propose that the dynamically unstable magnetic flux loops which are responsible for magnetic activity and mass loss in the form of "blobs" are also responsible for macroturbulent line broadening in the atmosphere of λ And. Thus the observed "line" is actually a superposition of many individual lines. As was noted above, the fact that discrete velocity features have been detected in certain RS CVn atmospheres (e.g. UX Ari, and λ And) already suggest that the features responsible for such velocity entities are macroscopic in size relative to the stellar disk. The stochastic nature of the velocity events (one occurs every time a new flux loop emerges at the surface) has the effect that the macroturbulent velocity field is by no means a constant feature of the atmosphere: this field is inherently time-dependent. Thus, there will occasionally be time periods when the macroturbulent parameter V_o will drop to values considerably less than the value of 30 km/sec mentioned above in our fitting of the profiles supplied by Bopp and Smith for four particular epochs. It is not surprising, therefore, that at times the macroturbulent broadening falls so low as to allow the central absorption dip to become visible in the core of the Ca K emission (cf. BD).

The interpretation of a velocity field characterized by a velocity parameter 30 km/sec in terms of magnetic "blobs" (or prominences) is still uncertain. In the Sun, flux loops appear to emerge with speeds of order $\lesssim$ 10 km/sec (Bruzek and Durrant, 1977). In fact macrotubulent broadening of precisely this order is required to reproduce observed Ca K lines in solar active regions (Shine and Linsky, 1974). Thus, our equating magnetic flux loop motions with macroturbulence is apparently consistent with detailed solar observations.

Since the velocity field in λ And is being ascribed to magnetic elements, it may be that there is a proportionality between V_o and the Alfven speed V_A in the atmosphere. For numerical purposes, we may refer to Fig. 9, and note that in one particular chromospheric model, there is a rather constant ion density over a rather broad range of mass loadings. If we use that constant density ($N_p \approx 10^{11}$ cm^{-3}) for purposes of estimating V_A, we find that $V_m/V_A \approx 4/B$ in the case of λ And (where B is the magnetic field strength in gauss). If the proportionality $V_m \propto V_A$ is valid, then stars with stronger fields will have larger macroturbulent broadening (other things being equal).

In this regard, we note that the system HR 1099, with a period of 2.8 days (and presumably synchronized axial-orbital rotation), has angular velocity some 20 times greater than λ And. Using the scaling $|B| \sim \Omega^{\alpha}$, where α = 1-1.5 (Kippenhahn, 1973), we expect that in HR 1099, V_A may exceed the value in λ And by at least 20. Scaling to the value of V_m, then, we find that macroturbulent broadening in HR 1099 may be characterized by a very large value (several hundred km/sec). This is consistent with the observations by

Weiler (1978), where, in HR 1099, features were observed in Mg k emission moving at up to ± 250 km/sec relative to the star. However, the proposed dynamo scaling $\beta \sim \Omega^{\alpha}$ must be treated with great skepticism: it is probably the total flux that scales with Ω, rather than the field strength. The latter may be determined by atmospheric processes.

Once again, it must be stressed that these are only consistency arguments at present. We cannot cite any definite evidence which proves that the macroturbulent velocity field which emerges from the line profile is certainly associated with the unstable arches of magnetic flux. But the evidence in favor of such an association is at least interesting enough to warrant further study.

Third Topic: (IV) STL crossing and T Tau phenomena

We have combined empirical estimates of chromospheric pressures in T Tau stars with various estimates for their masses and radii in order to determine whether these stars lie above or below the STL. We have found that indeed, the empirical data are consistent with the stars being above the STL, but only marginally. Our discussion above suggests that we modify our notation, and instead discuss the T Tau phenomenon in terms of MTTL, rather than STL. The conclusion remains unchanged: the T Tau stars lie close to, but probably above, the MTTL. Hence, just as for the RS CVn stars, we claim that their atmospheres are in a state of continual magnetic upheaval because magnetic flux loops can find no static equilibria. Hence, if our interpretation of macroturbulent line broadening in the RS CVn stars is correct, we expect that the T Tau stars should also show large macroturbulent broadening. In fact, a very recent study (Herbig and Soderblom, 1980) has shown extremely large macroturbulent broadening velocities in many of the T Tau stars: values of 45-100 km/sec have been derived by Herbig and Soderblom for some of the stars. It is true that in the case of these stars, we are not in the fortunate situation (as we were with λ And) of being able to exclude definitely the effects of axial rotation in contributing to the macroturbulent line broadening. However, we note that, analogous to some of the RS CVn stars, individual elements have been observed in the line profiles of certain T Tau stars (e.g. YY Ori; Walker and Burstein, 1980) moving with speeds of up to ± 200 km/sec relative to the star. Rotation can presumably not give rise to such high speed, variable-in-time entities, whereas flux-loop emergence of the kind we discuss here is a viable candidate to explain these "features" in the line profiles. Again, therefore, we are led to propose that the macroturbulence in T Tau stars can be ascribed to magnetically unstable loops lifting off the surface.

The T Tau stars are believed to be young. Therefore, their evolution in the HR diagram is probably still from right to left. Thus, they are approaching the MTTL from the right hand side. This is the opposite sense to the RS CVn stars (which are evolving toward the red-giant region). Thus, it is partially a coincidence that the active stars in the RS CVn stars and the T Tau stars lie close to the MTTL. In that sense, therefore, it was a coincidence which allowed Hall (1972), in his first paper on RS CVn itself, to use the epithet "T Tau like" to describe the phenomena in the active star of the RS CVn system.

According to our interpretation, the activity and mass loss process in the T Tau stars should soon be stopping as the star evolves further to the left in the HR diagram, and falls eventually below the MTTL. In this regard, it is interesting to note that some of the T Tau stars are observed to contain apparently infalling matter in their atmospheres from time to time. The infalling matter is by no means always present (Walker and Burstein, 1980, and references), and in fact at other times, a star previously classified as an infalling star (a "YY-Orionis object"), may show undisputed evidence for outflow (Herbig 1977; Ulrich and Knapp, 1980). We can readily understand these in/out events in terms of closeness to the MTTL. Thus, at a certain time, coronal heating may be such that the sonic point lies below 2 R_{star}, and so magnetic loops are unstable, and begin to evolve outward. At a later time, conditions may have changed slightly, so that the sonic point moves out beyond 2 R_{star}. Then, at any one time, layers in the atmosphere may be expanding away from the star, while other layers may be falling back. This is consistent with the data (Walker and Burstein, 1980; Edwards, 1979). These on/off events should be a feature of stellar evolution as long as the star is close to the MTTL.

If the macroturbulent velocities can be interpreted as being proportional to V_A, then the larger values of macroturbulence in T Tau stars than in RS CVn stars suggests that the V_A values are higher in the T Tau stars. The fact that in YY Ori, "blobs" were observed to be moving relative to the star with speeds comparable to those seen in HR 1099 might suggest that V_A in these two stars may be similar.

Fourth Topic: (II) Starspots

Observational evidence for the temperatures in starspots on different classes of stars has been accumulating rapidly recently. The most direct estimate of temperatures in the spot presumably refer to the penumbrae of the spot (if the umbra/penumbra division is valid), simply because of enhanced emission intensity at the hotter penumbral temperatures. Then, conversion to an umbral temperature is more uncertain.

For the RS CVn-type system II Peg, Vogt (1980) has recently obtained temperatures by two methods. One involves subtraction spectrophotometry, which gives him the spectrum of the spot, from which a spectral class can be estimated from the molecular features: this leads to M6 spectral type, corresponding to 2800 K, i.e. ΔT_{pen} is 1800 K cooler than the photosphere. The second method is based on broad-band photometry, and leads to $\Delta T_{pen} = -1200$ K relative to the photosphere. At a different epoch, Bopp and Noah (1980) used multicolor photometry for the same star and found $\Delta T_{pen} = -1200$ K also. It is not clear why the spectrophotometric method gave a much cooler penumbra. Vogt went on to estimate what the umbral temperature might be by simply scaling from the sun. He referred to the ratio $\mu = T(umbra)/T(penumbra)$ which in the sun is about 0.76. He proposed that if μ retains this value in other stars,

then his data suggest that the umbral temperature in II Peg is some 2000-2500 K cooler than the photosphere.

For the RS CVn star λ And, Bopp and Noah (1980) found ΔT_{pen} = -800 K in 1977, but a much larger value, -2000 K, in 1976. The latter value is somewhat uncertain, but it corresponds (applying the μ-scaling above) to an umbral cooling ΔT_{umb} = -2700 K.

For the active star in HR 1099 (which may be a main sequence star), Dorren and Guinan (1980) found ΔT_{pen} = -1800 K, from multicolor photometry. Applying the μ-scaling, then this leads to ΔT_{umb} = -2800 K. On the same star, Ramsey and Nations (1980) have obtained spectrophotometry of the spotted hemisphere of sufficient quality to allow them to identify a spectral type for the spotted hemisphere. From this, they conclude that ΔT_{pen} is at least as large as 10^3 K. Applying the μ scaling to this result, we find ΔT_{umb} to be at least -2100 K.

These studies all point in the direction of much larger empirical values for the umbral cooling than was hitherto believed. Thus, the correction to the starspot models of Mullan (1974) may be much smaller than suspected when the present proposal was originally written. In fact, Vogt (1980) has referred to my earlier models in order to obtain a crude estimate of the magnetic field strength in II Peg. The result is 3 kG. This procedure is of course not strictly correct, because my models were computed for a dwarf star, where II Peg has a gravity that is closer to a subgiant. Nevertheless, Vogt's idea of using effective temperatures of starspot models for purposes of estimating magnetic field strengths in RS CVn stars is an exciting one, as long as no direct observational methods have succeeded in measuring the fields. Hence, more detailed modelling of a spot in a star of correct gravity for the RS CVn systems will represent a worthwhile investment of research effort even if detailed corrections for Alfven wave reflection and heating cannot be parametrized exactly at the present time.

References

Ahmad, I. A. and Webb, D. F. 1978, Solar Phys. 58, 323.

Ayres, T. R., Linsky, J. L., Vaiaba, G. S., Golub, L., and Rosner, R. 1980, Bull. Amer. Astron. Soc. 12, 870.

Baliunas, S. L. and Dupree, A. K. 1979, Ap. J. 227, 870 (BD).

Baliunas, S. L., Avrett, E. H., Hartmann, L. and Dupree, A. K. 1979, Ap. J. Letters 233, L 129.

Bell, R. A. and Gistaffson, B. 1980, private communication.

Bopp, B. W. and Talcott, J. 1978, Astron. J. 83, 1517.

Bopp, B. W. and Noah, P. V. 1980, Publ. Astron. Soc. Pacific 92, 717.

Bruzek, A. and Durrant, C. J., 1977, Illustrated Glossary for Solar and Solar-Terrestrial Physics (Dordrecht: Reidel), p. 57.

Cram, L. E. and Mullan, D. J. 1979, Ap. J. 234, 579.

Davis, J. M. 1980, Bull. Amer. Astron. Soc. 12, 518.

Dorren, J. D. and Guinan, E. F. 1980, Bull. Amer. Astron. Soc. 13, 452.

Edwards, S. M. 1979, Publ. Astron. Soc. Pacific, 91, 355.

Gibson, D. M. 1977, Bull. Amer. Astron. Soc. 9, 600.

Gingerich, O. and Rich, J. 1969, in Theory and Observations of Normal Stellar Atmospheres (MIT Press), p. 408.

Gray, D. F. 1976, Observation and Analysis of Stellar Photospheres, (New York: Wiley), p. 422.

Habbal, S. R. and Withbroe, G. L., 1980, Solar Phys. (in press).

Hall, D. S., 1972, Publ. Astron. Soc. Pacific, 84, 323.

Hall, D. S., 1978, Astron. J. 83, 1469.

Herbig, G. H. 1977, Ap. J. 214, 747.

Herbig, G. H. and Soderblom, D. R. 1980, Ap. J. 242, 628.

Holzer, T. E., 1980, Smithsonian Ap. Obs. Spec. Rep. #389, p. 153.

Kippenhahn, R., 1973, in "Stellar Chromospheres", Proc. IAU Colloq. No. 19, eds. S. Jordan and E. Avrett (Washington: NASA SP-317 p. 275.

Kopp, R. A. and Holzer, T. E., 1976, Solar Phys. 49, 43.

Kraft, R. P., Preston, G. W., and Wolff, S. C., 1964, Ap. J. 140, 235.

Leer, E. and Holzer, T. E., 1980, J. Geophys. Res. 85, 4681.

Levy, E. H. and Rose, W. K., 1975, Ap. J. 193, 245.

Linsky, J. L. and Haisch, B. M., 1979, Ap. J. Letters 229, L27.

Low, B. C., 1980, Bull. Amer. Astron. Soc. 12, 902.

Lutz, T. E., 1970, Astron. J. 75, 1007.

Mullan, D. J., 1974, Ap. J. 192, 149.

Mullan, D. J., 1978, Ap. J. 226, 151.

Mullan, D. J., 1980, Smithsonian Ap. Obs. Spec. Rep. #389, p. 189.

Munro, R. H. and Jackson, B. V., 1977, Ap. J. 213, 874.

O'Brien, G., 1980, Bull. Amer. Astron. Soc. 12, 747; also Ph.D. dissertation, Univ. of Texas, Austin.

Paczynski, B., 1970, Acta. Astron. 20, 47.

Pneuman, G. W., 1968, Solar Phys. 3, 578.

Popper, D. M., 1970, IAU Colloq. No. 6, p. 13.

Popper, D. M. and Ulrich, R. K., 1977, Ap. J. Letters 212, L131.

Ramsey, L. and Nations, H. L., 1980, Ap. J. Letters 239, L121.

Sheeley, N. R. and Golub, L., 1979, Solar Phys. 63, 119.

Shine, R. A. and Linsky, J. L., 1974, Solar Phys. 39, 49.

Simon, T., Linsky, J. L. and Schiffer, F. H., 1980, Ap. J. 239, 911.

Stencel, R. E. and Mullan, D. J., 1980, Ap. J. 238, 221; addendum, ibid. 240, 718.

Swank, J. H. and White, N. E., 1980, Smithsonian Ap. Obs. Spec. Rep. #389, p. 47.

Ulrich, R. K. and Knapp, G. R. 1979, Ap. J. Letters 230, L99.

Vernazza, J. E., Avrett, E. H. and Loeser, R., 1980, Ap. J. Suppl. (in press).

Vogt, S. S., 1980, preprint.

Walker, M. F. and Burstein, D., 1980, Publ. Astron. Soc. Pacific, 92, 648.

Wallenhorst, S. G., 1980, Ap. J. 241, 229.

Weiler, E. J., 1978, Astron. J., 83, 795.

Wilson, O. C. and Bappu, M.V.K., 1957, Ap. J. 125, 661.

Wilson, O. C., 1973, in "Stellar Chromospheres" Proc. IAU Colloq. No. 19, eds. S. Jordan and E. Avrett (Washington: NASA SP-317) p. 310.

Zahn, J. P., 1977, Astron. Ap. 57, 383.

Figure Captions

Figure 1. Portion of the HR diagram where various "dividing lines" have been discovered. Rapid mass loss sets in when a star crosses above the velocity dividing lines represented by Mg and Ca asymmetries. Hot material disappears from the atmospheres when a star evolves upwards across the lines labelled Coronae and X-rays.

Figure 2. (Above) Mg asymmetry in sample of 10 subgiants. S/L denotes ratio of shortward to longward intensities in the doubly reversed emission of Mg II h and k. S/L < 1 denotes rapid mass loss, which sets in at K0-K1 for these stars.
(below) Distribution of spectral types for active secondary stars in RS CVn systems. Note concentration among early K subgiants.

Figure 3. Scenario for mass loss driven by magnetic reconnection. This predicts mass loss which is neither spherically symmetric nor steady in time. The mass loss process is supposed to occur by means of a random succession of events of the type shown above.

Figure 4. Expansion of bubble rising through the solar corona. Bubble size is expressed in terms of angle subtended at sun center (right-hand scale). Solid line assumes that bubble material equilibrates its density with the ambient density. Dashed line: empirical determination of coronal hole boundary (left-hand scale). We propose that mass loss in solar corona holes occur in the form of a succession of bubbles, each of which expands in the above fashion, thereby determining the gross expansion properties of coronal holes.

Figure 5. Dividing lines in the HR diagram: VDL (TDL) denote velocity (temperature) dividing lines. Data from which VDL was derived are shown for individual stars, depending on whether there is rapid mass loss (S/L < 1) or not. Theoretical MTTL occurs at the circled T's. The old STL lies at the circled P's. Note that empirical VDL agrees well with MTTL; suggesting that rapid mass loss sets in when magnetic field loops open up.

Figure 6. $H\alpha$ line profiles computed with isothermal chromospheres superposed on the models of GR. The model in (e) will be used below to add more realistic chromospheric temperature rises.

Figure 7. $H\alpha$ line profile computed with an isothermal chromosphere superposed on a model of Bell and Gustaffson (1980). This is to be compared with Fig. 6(e) above: There is no essential difference between the profiles.

Figure 8. Chromospheric temperature structures which have been adopted in the present work. Photospheric model has T_e = 5000 K and log g = 3.0. An empirical solar model is shown for comparison.

Figure 9. Variations of certain parameters with altitude in one of the converged model chromospheres. N_p denotes proton number density, N_H represents total number density of hydrogen nuclei.

Figure 10. Profiles of Hα computed using the chromospheric models whose temperature structures are shown in Figure 8.

Figure 11. (half of) observed Hα profiles in λ And at 4 epochs (courtesy of B. W. Bopp and S. Smith). These are smoothed profiles; original data extend much farther from line center than the segments shown here.

Figure 12. Effects of macroturbulent broadening on Hα lines in four models. All models have the same photosphere (T_e = 5000 K, log g = 3.0). (i) isothermal chromosphere; cf. Figure 6(e); (ii)-(iv) cf. profiles shown in Figure 10 in unbroadened form. Curves are labelled with the velocity parameter (km/sec) which characterizes the Gaussian velocity distribution of the macroturbulent elements.

Figure 13. Attempted fit of a broadened profile with one of Bopp and Smith's observed profiles.

Personnel

The Principal Investigator attended the following scientific meetings during the reporting period.

(i) Cool Star Workshop, Harvard College Observatory, January 31, 1980.

(ii) American Astronomical Society Meeting, College Park, Maryland June 17, 1980.

(iii) Workshop on Physical Processes in Red Giants, Erice, Sicily September 3-10, 1980.

The P.I. visited Sacramento Peak Observatory (March 3-8, 1980) for discussions with Dr. L. E. Cram concerning adapting our chromospheres modelling program for the RS CVn systems.

The following talks were presented.

(i) "Non-thermal Stellar Winds in Cool Stars", presented at the Cool Star Workshop, Harvard College Observatory, January 31, 1980.

(ii) "Heating of Stellar Chromospheres and Coronae", colloquium at Armagh Observatory, N. Ireland, August 22, 1980.

(iii) Mass Loss from Warm Giants: Magnetic Effects", presented at the Erice Workshop on Red Giants, September 7, 1980.

(iv) "Chromospheres and Coronae among Cool Giants", presented to Delaware Astronomical Society, November 19, 1980.

(v) "Mass Loss from Coronal Holes driven by Magnetic Reconnection", (with I. A. Ahmad), American Astronomical Society, Solar Physics Division Meeting, Taos, New Mexico, January 10, 1981.

The following papers were published, or submitted for publication.

(i) Non-thermal Stellar Winds in Cool Stars, Smithsonian Astrophysical Observatory Special Report No. 389 (ed. A. K. Dupree), p. 189.

(ii) Magnetic Reconnection and Rapid Mass Loss in Cool Giants, submitted to Ap. J. Letters.

(iii) Heating of Chromospheres and Coronae in Cool Stars, Irish Astron. Journal (in press).

(iv) Mass Loss from Warm Giant Stars: Magnetic Effects, Proceedings of Erice Workshop on Red Giants. (eds. I. Iben and A. Renzini), (Dordrecht: Reidel), p. 355 (in press).

(v) Coronal Holes: Mass Loss Driven by Magnetic Reconnection, (with I. A. Ahmad), submitted to Solar Physics.

(vi) Onset of Rapid Mass Loss from Giants: Transition from Static to Dynamic Magnetic Fields, submitted to Ap. J.

In December, an advertisement for a candidate for the Postdoctoral Position for which second year funds were allocated was placed with the job service of the American Astronomical Society, and also in Physics Today. So far, three candidates have responded, and one of these looks promising. A decision is expected to be taken concerning one of these candidates sometime in the next few months.

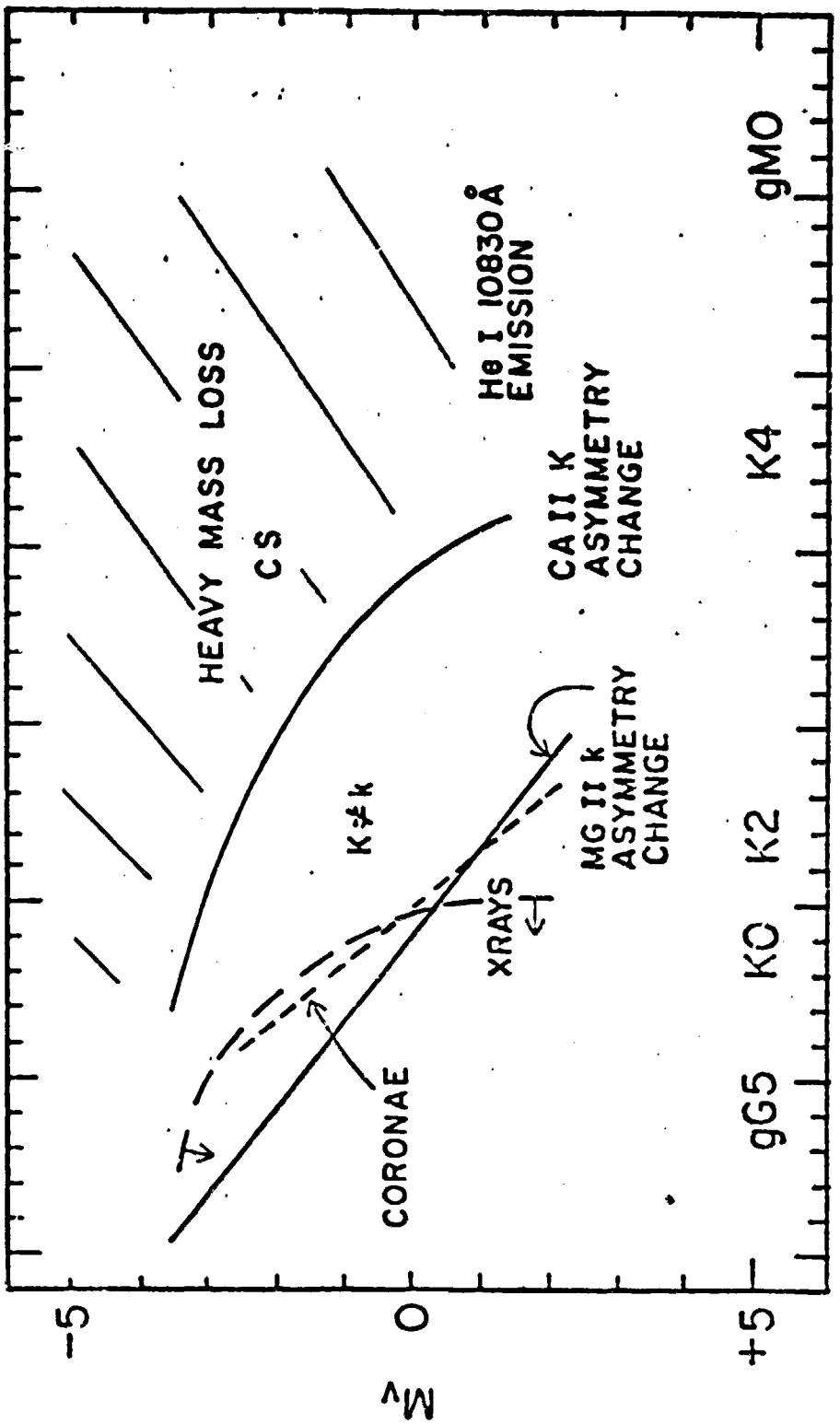

Fig. 1

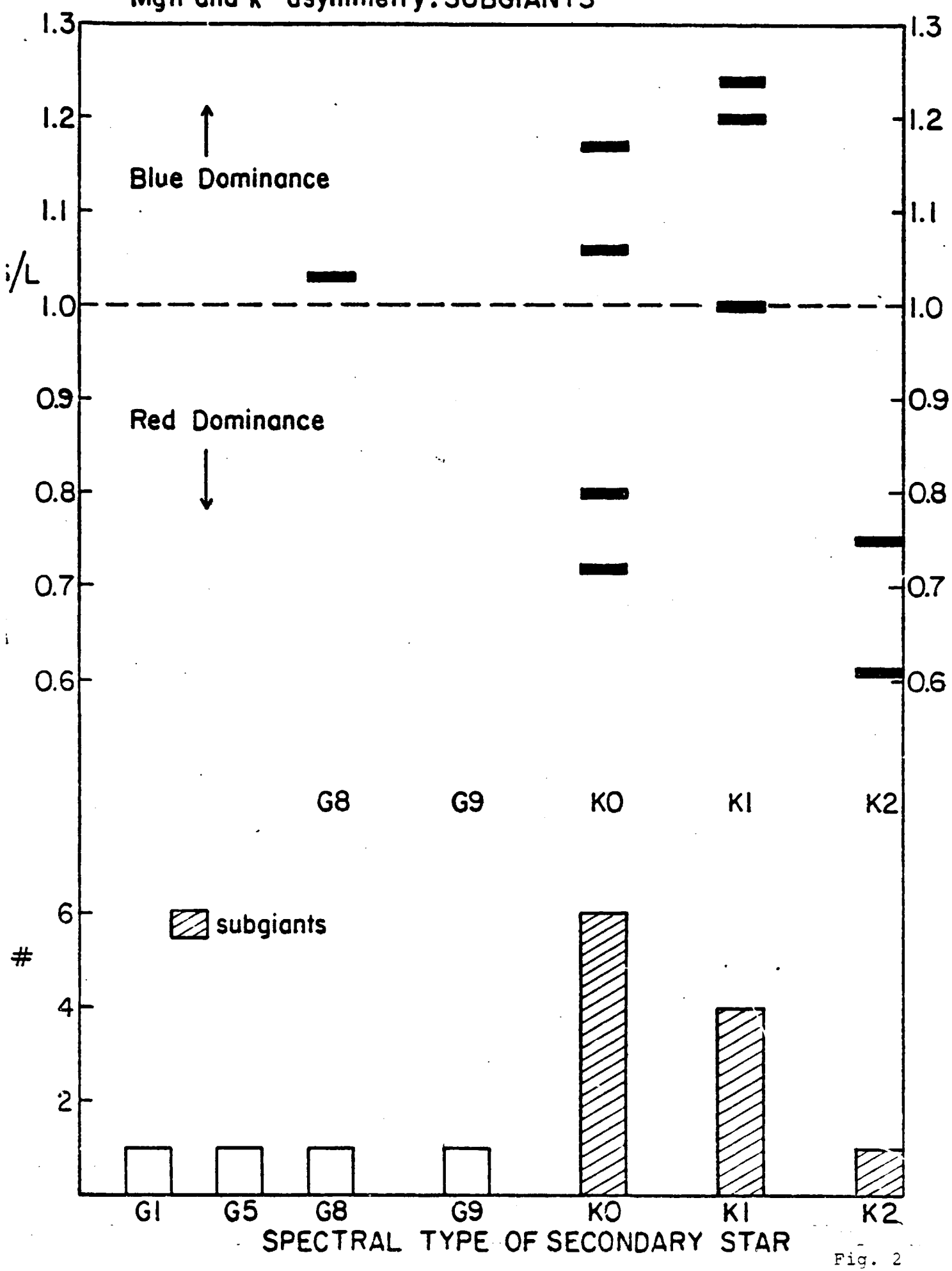
Mgh and k asymmetry: SUBGIANTS
1.3
1.2
1.1
1.0
0.9
0.8
0.7
0.6
i/L
Blue Dominance
Red Dominance
G8
G9
KO
KI
K2
6
4
2
#
subgiants
G1
G5
G8
G9
KO
KI
K2
SPECTRAL TYPE OF SECONDARY STAR

Fig. 2

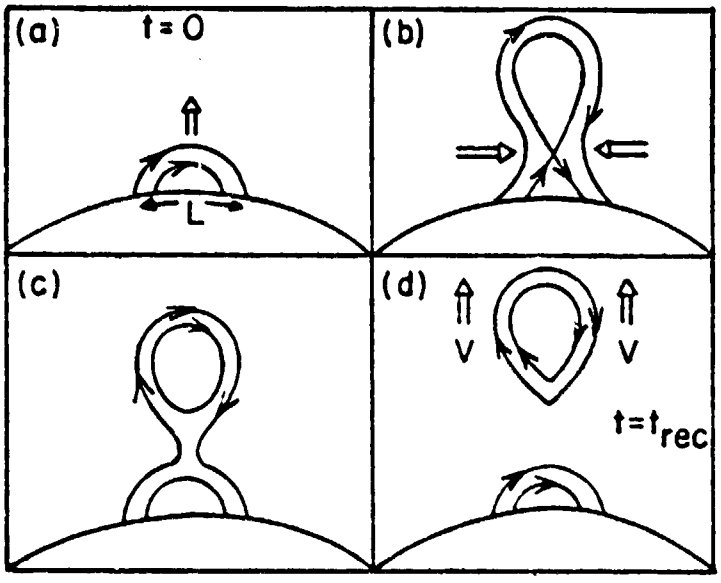

Fig. 3

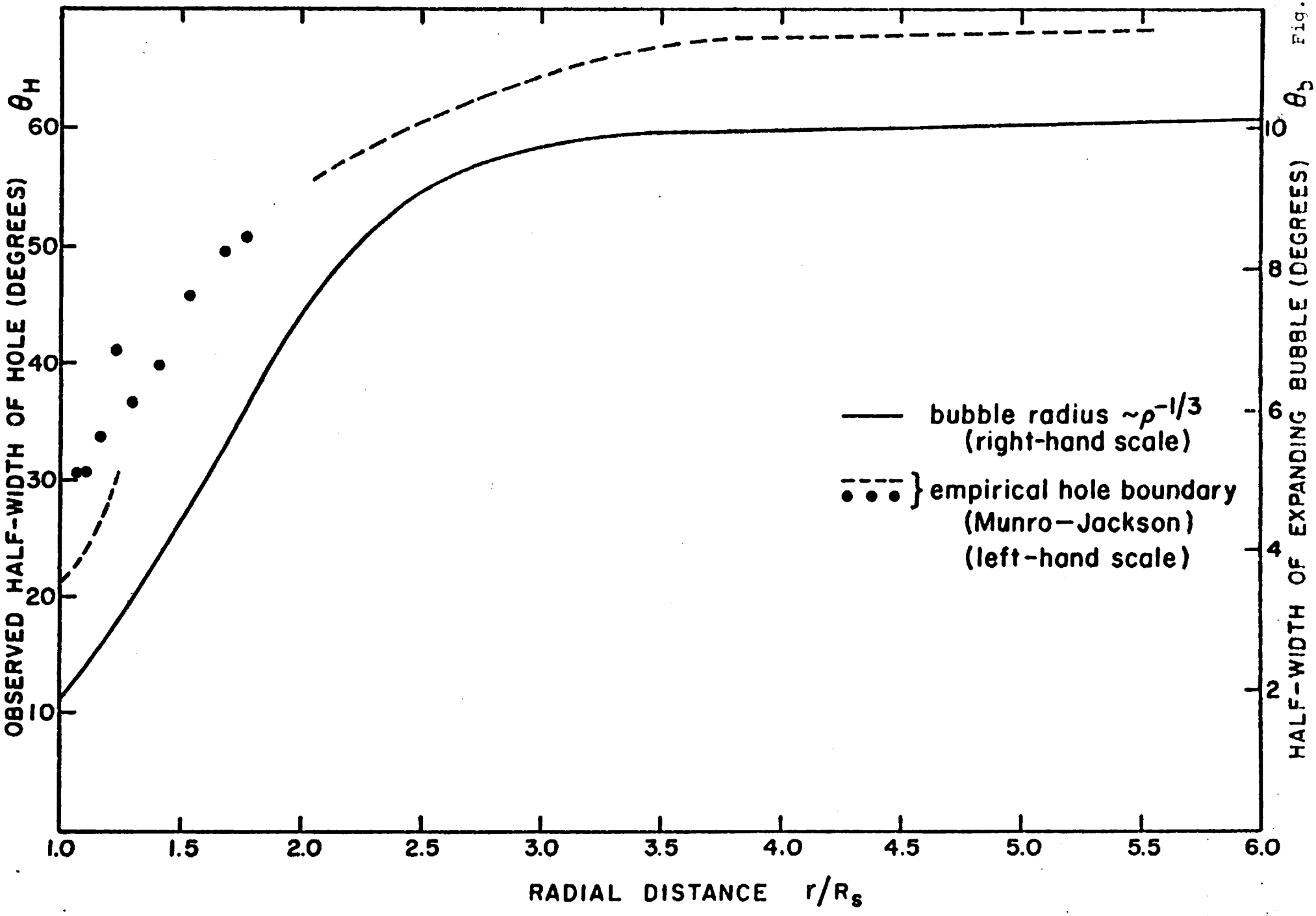
OBSERVED HALF-WIDTH OF HOLE (DEGREES) θ_H
HALF-WIDTH OF EXPANDING BUBBLE (DEGREES) θ_b
RADIAL DISTANCE r/R_s
10
20
30
40
50
60
2
4
6
8
10
1.0
1.5
2.0
2.5
3.0
3.5
4.0
4.5
5.0
5.5
6.0
bubble radius $\sim\rho^{-1/3}$
(right-hand scale)
empirical hole boundary
(Munro–Jackson)
(left-hand scale)

Fig. 4

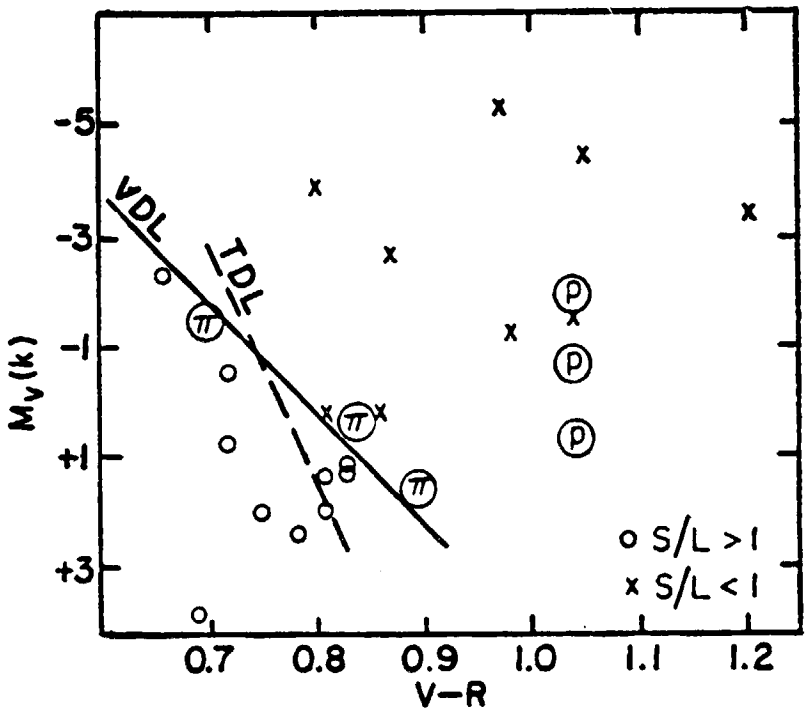

Fig. 5

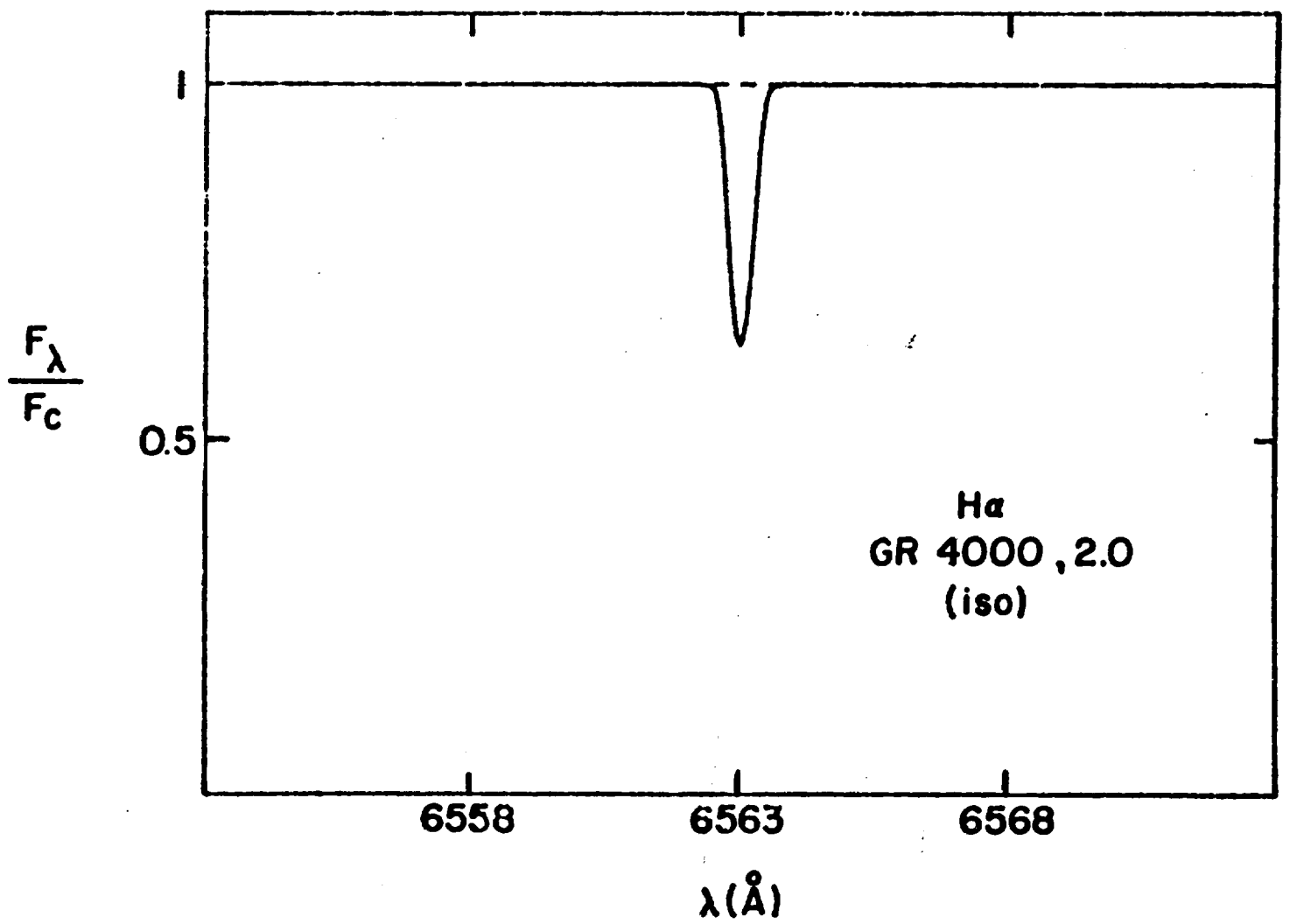

Fig. 6(a)

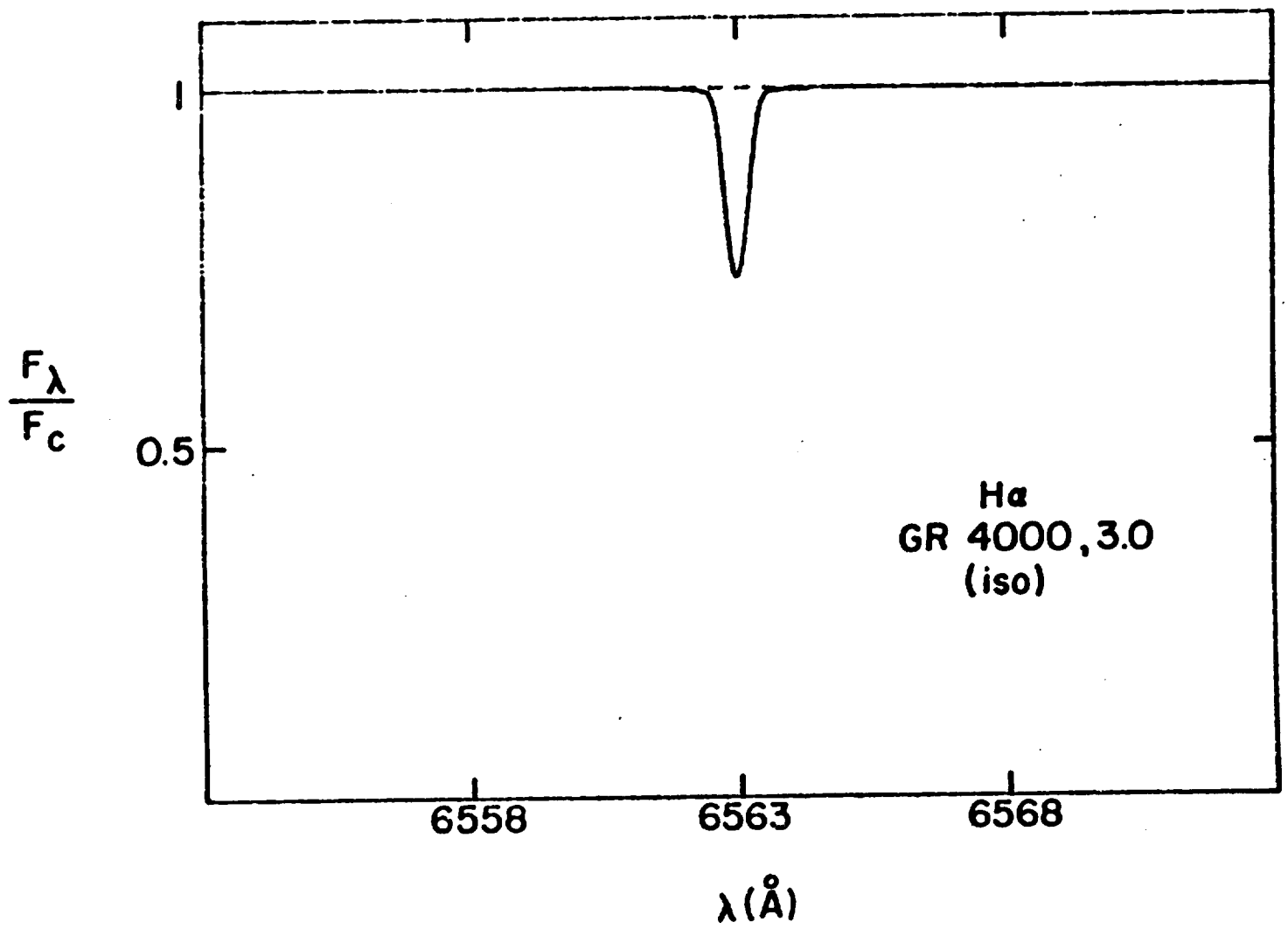

Fig. 6(b)

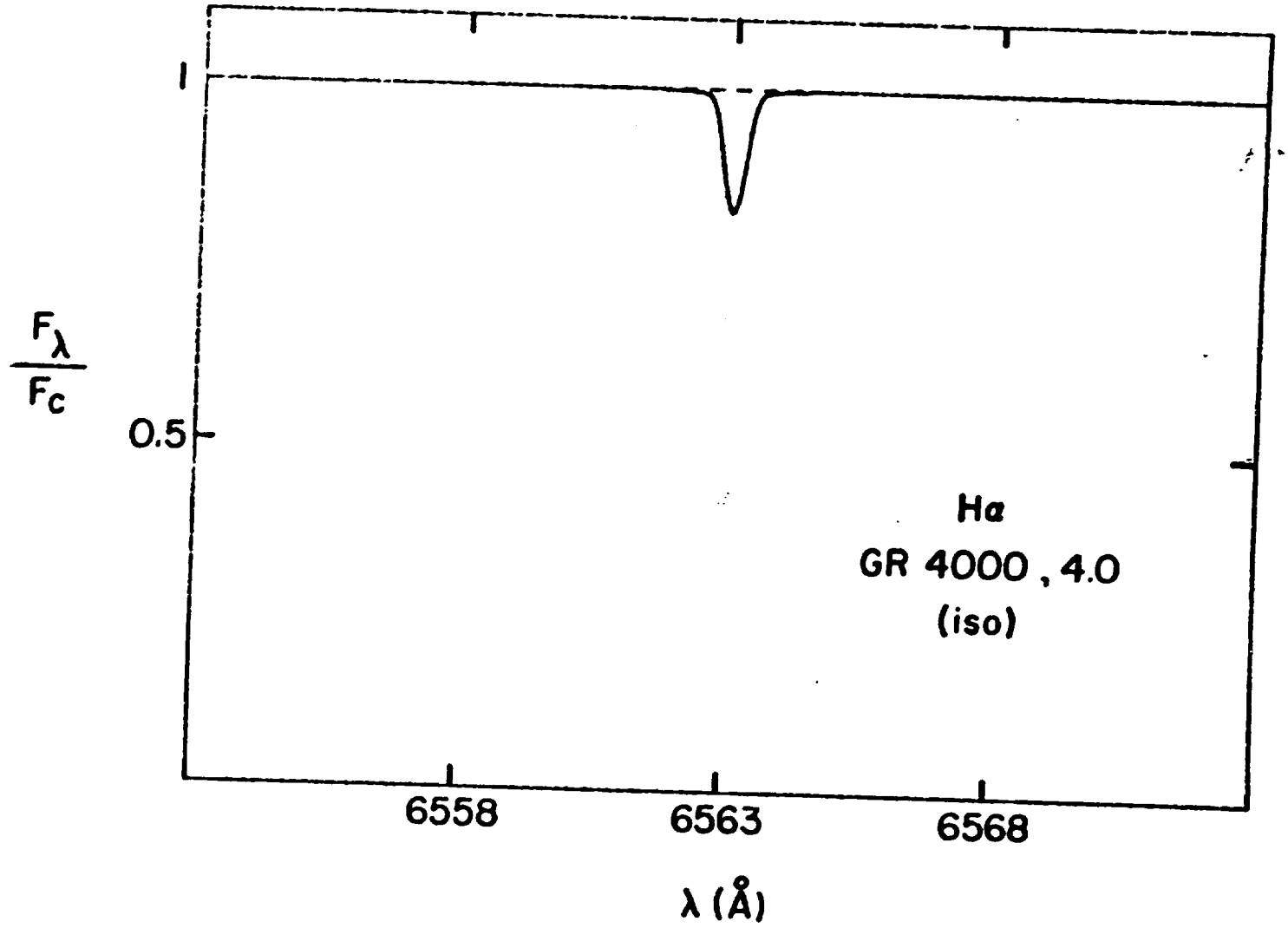

Fig. 6(c)

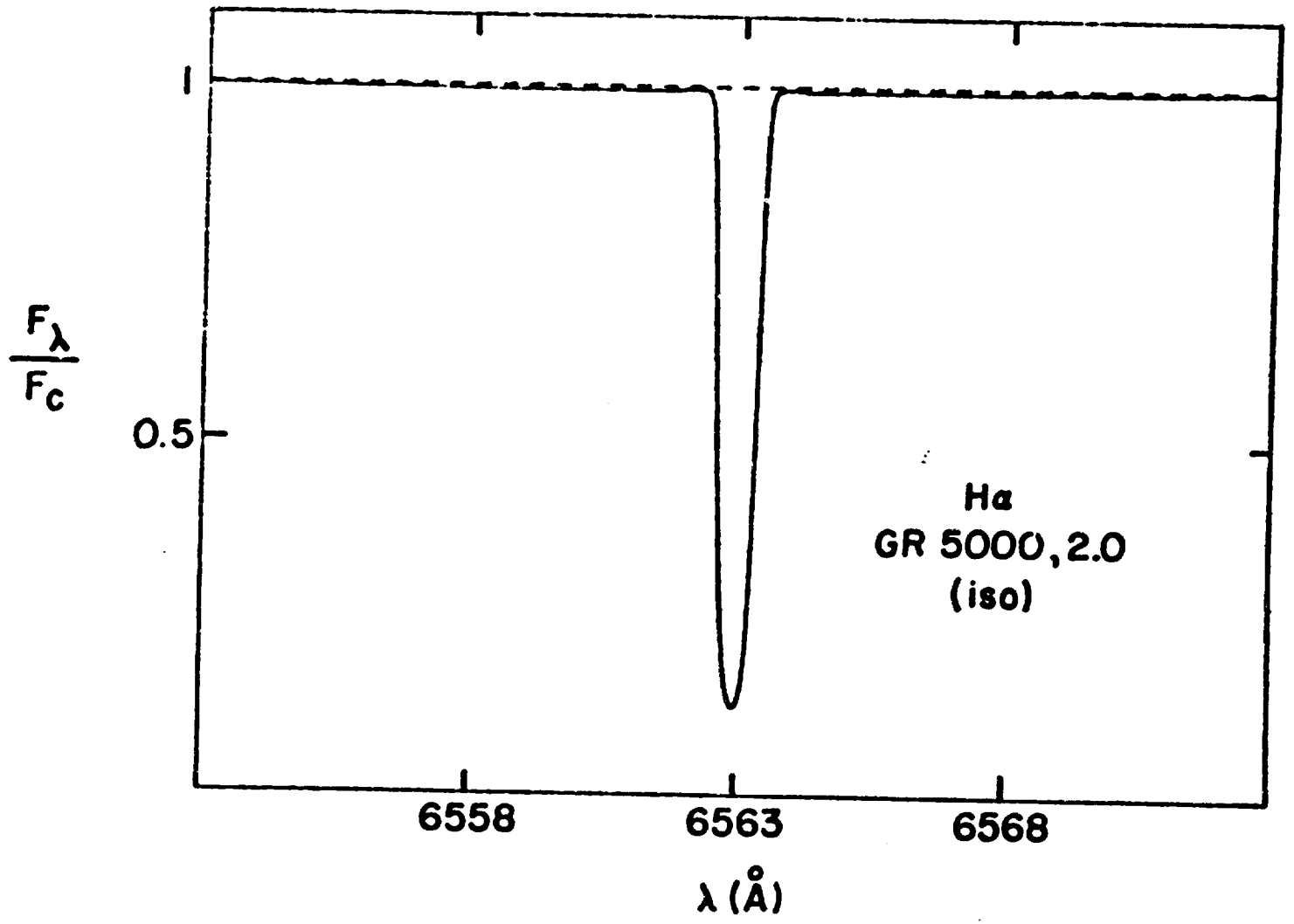

Fig. 6(d)

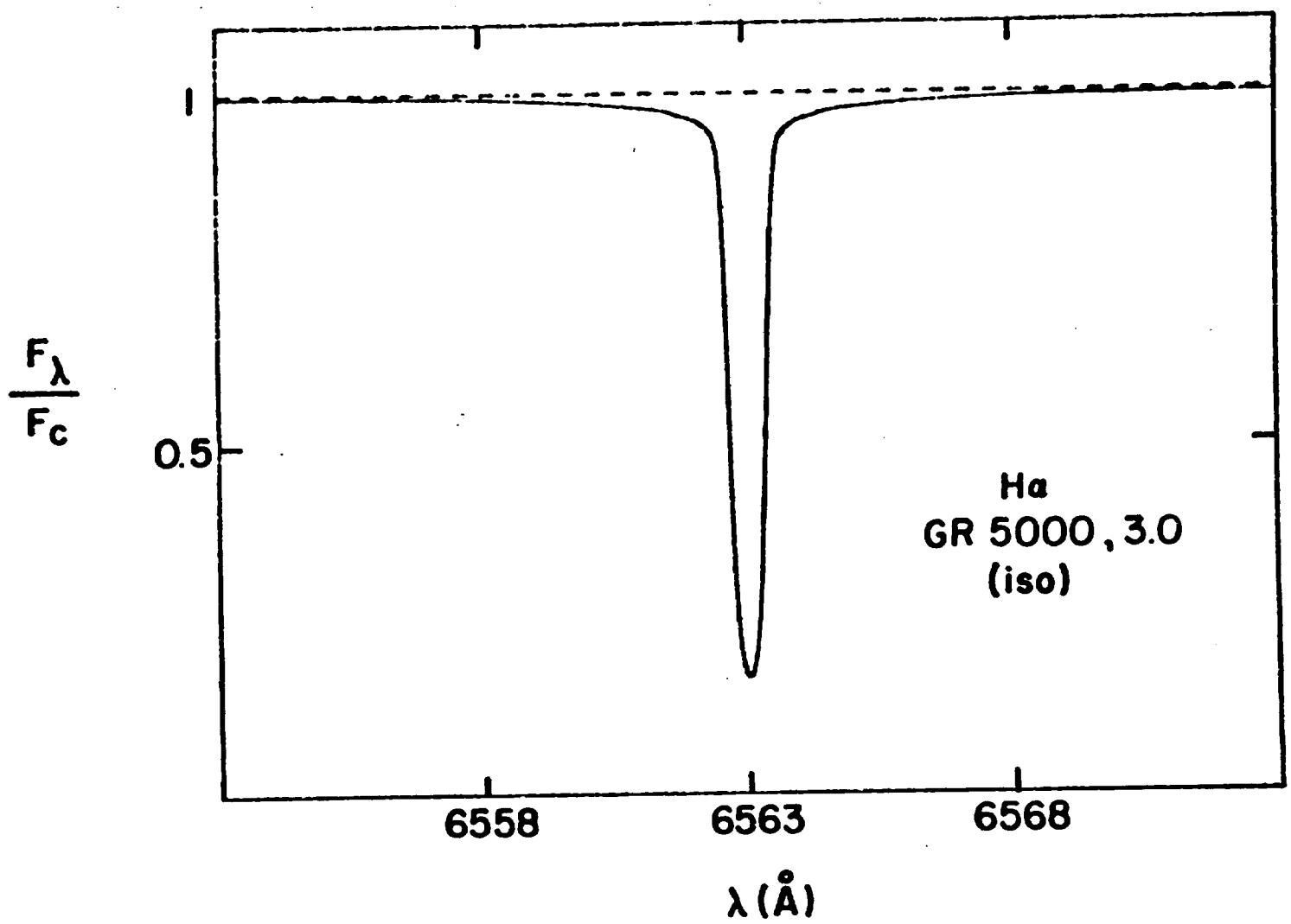

Fig. 6(e)

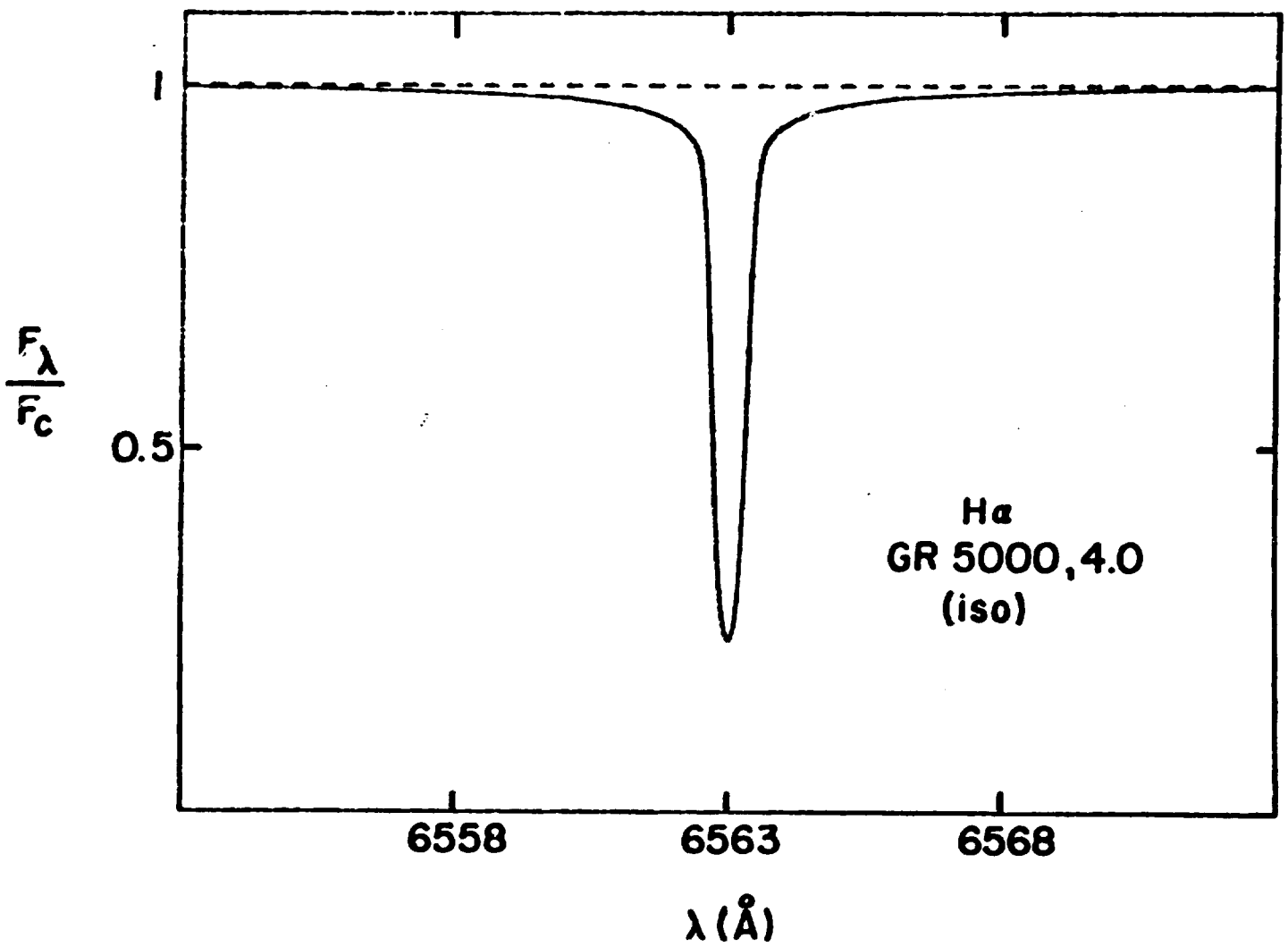

Fig. 6(f)

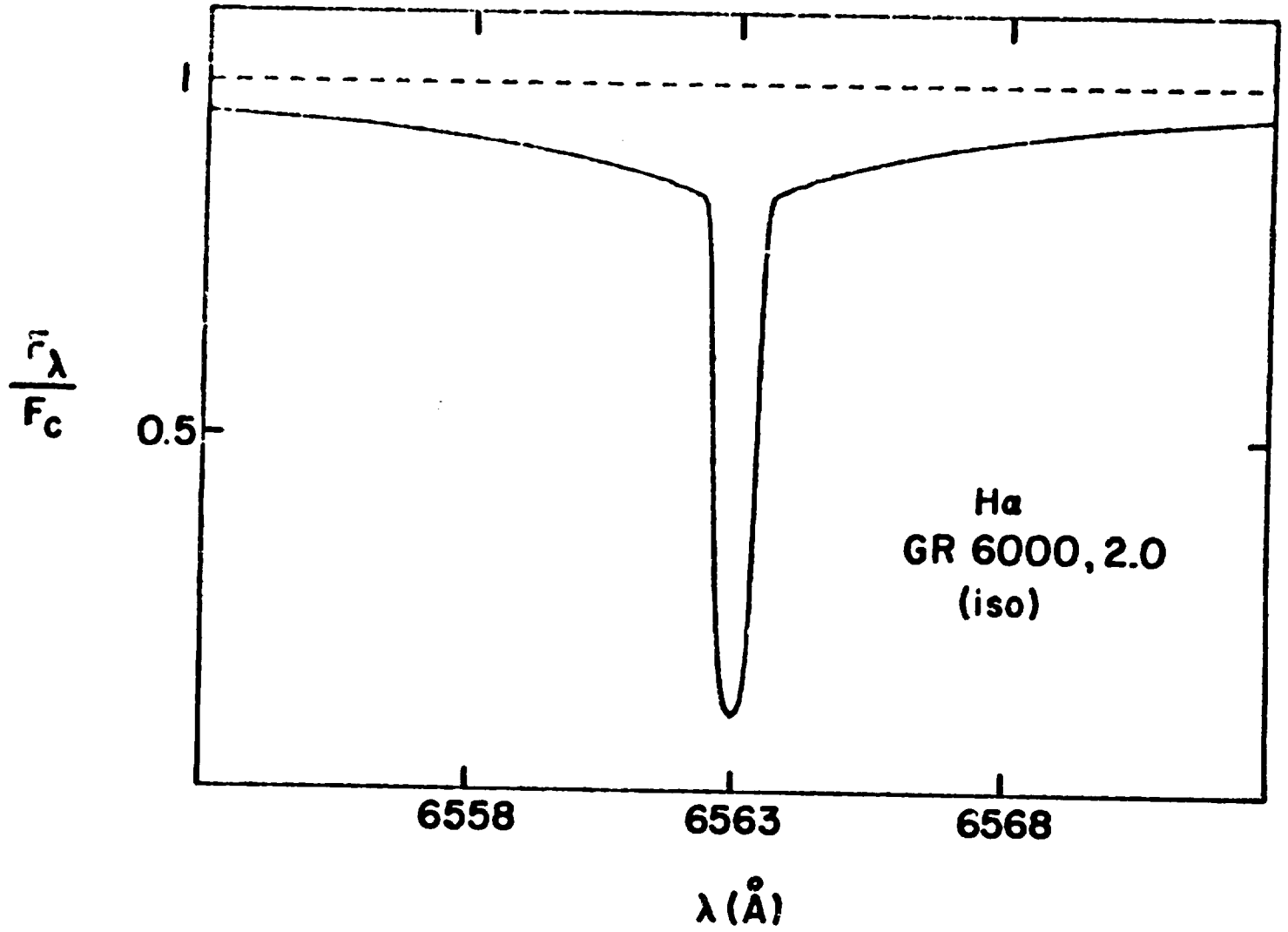

Fig. 6(q)

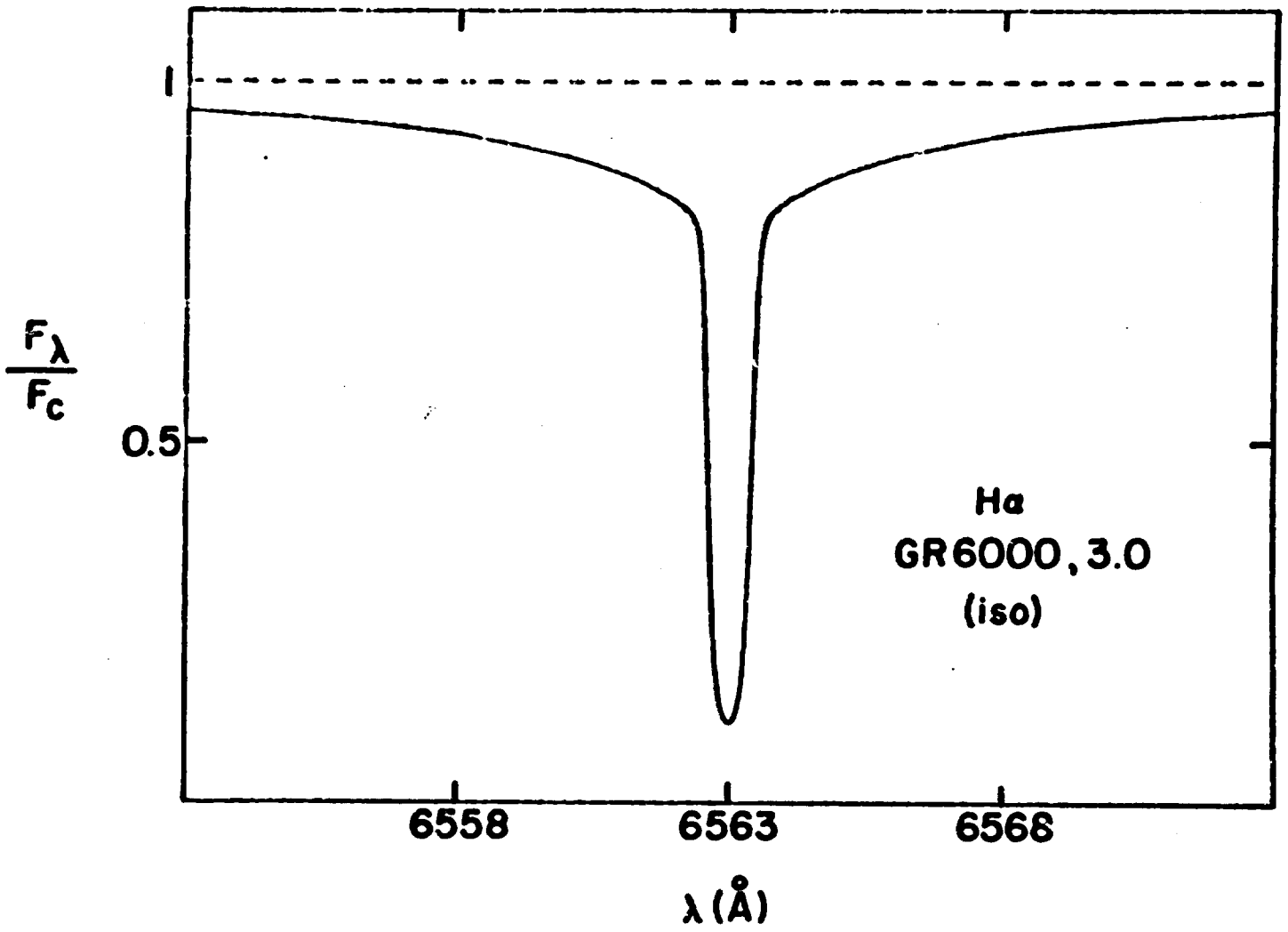

Fig. 6(h)

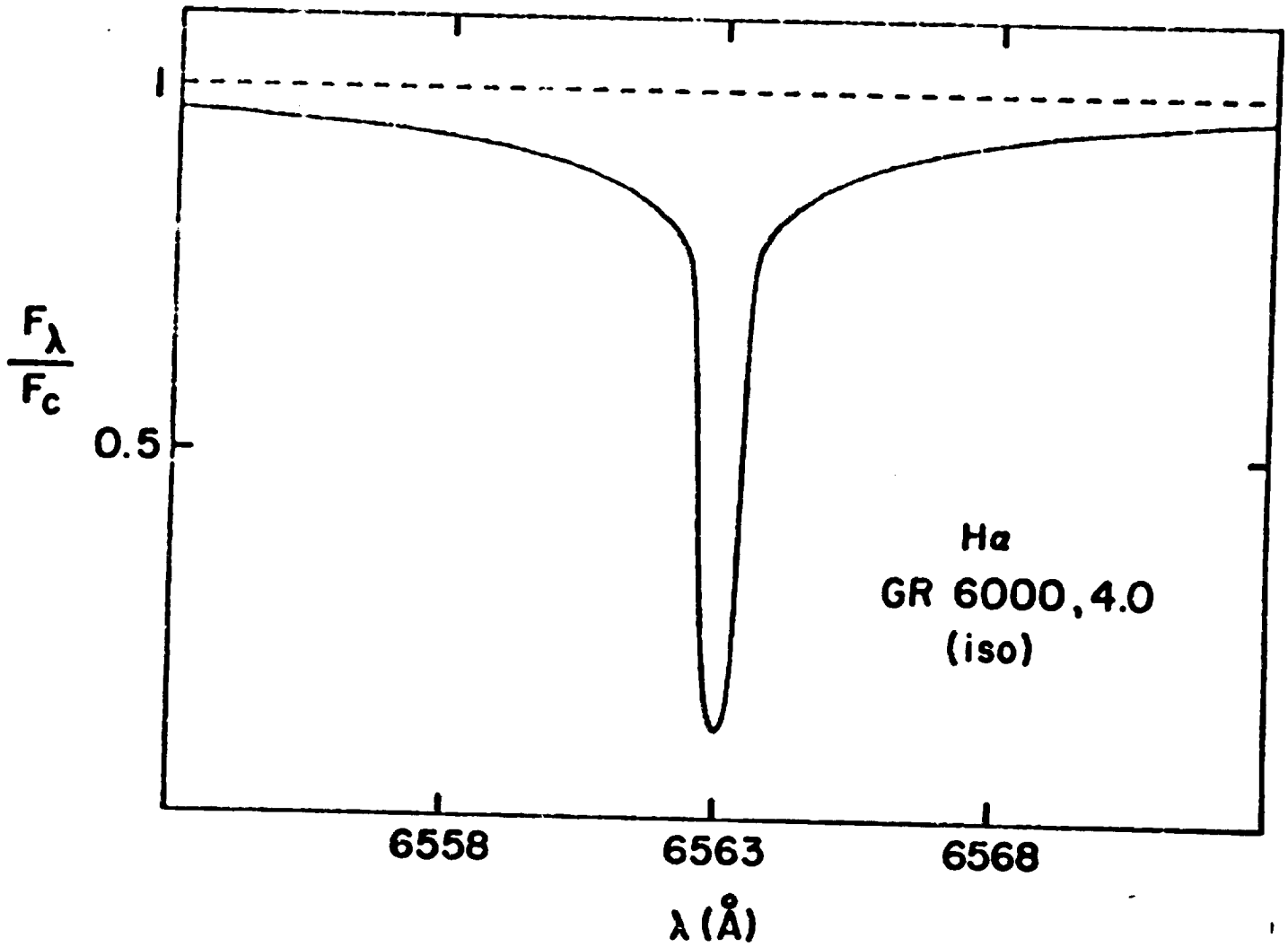

Fig. 6(i)

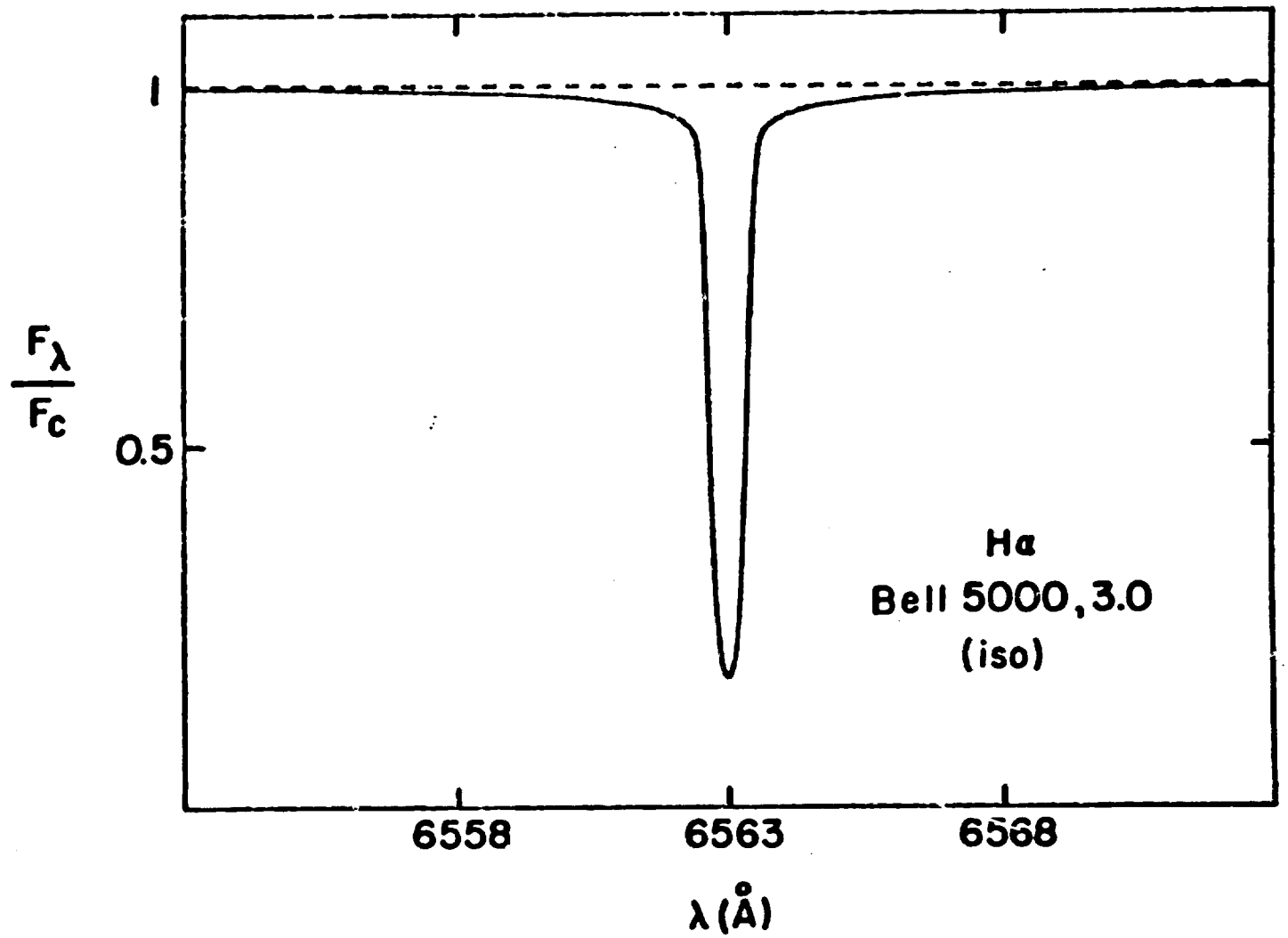

Fig. 7

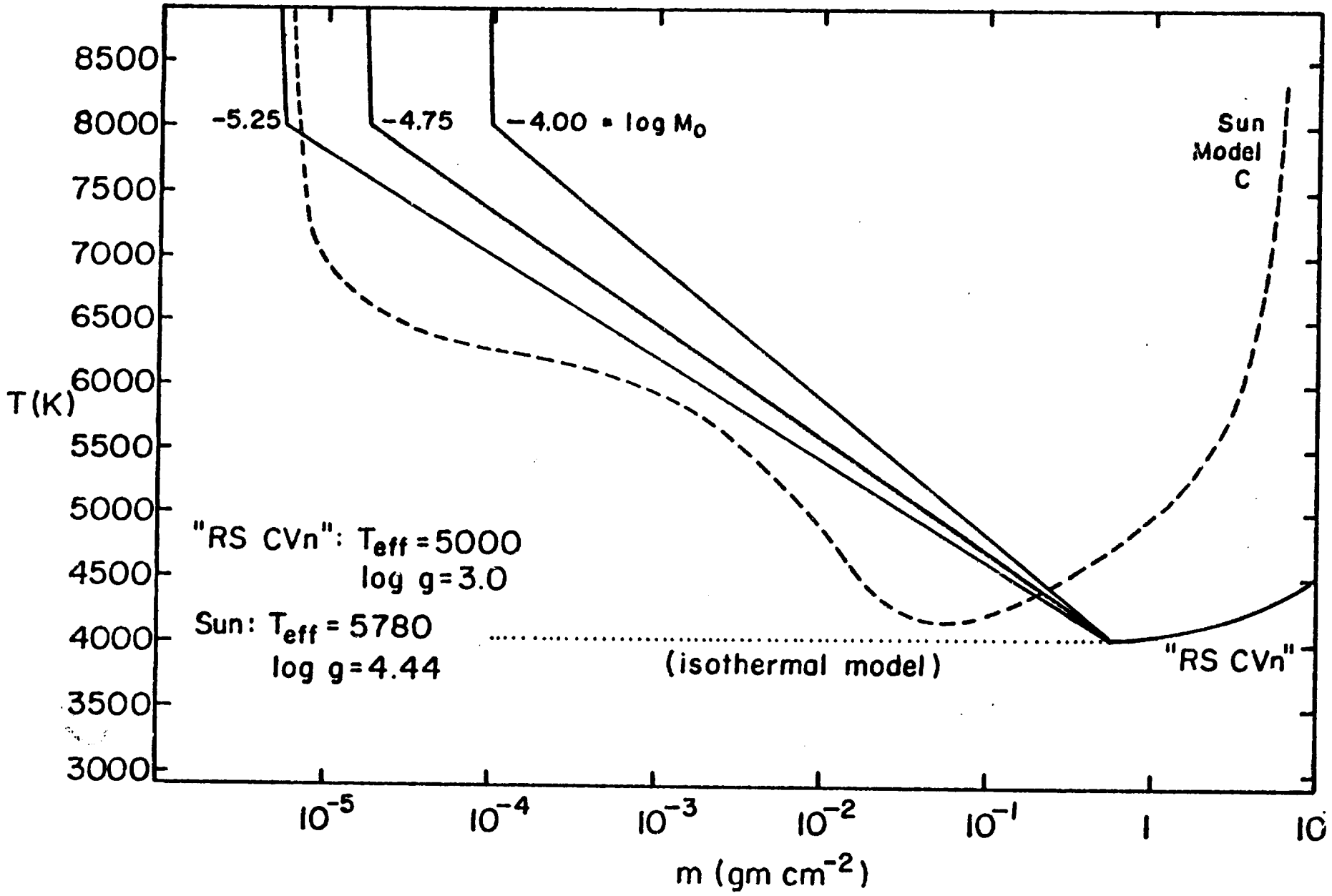
8500
8000
7500
7000
6500
6000
5500
5000
4500
4000
3500
3000
T(K)
-5.25
-4.75
-4.00 • log M₀
Sun
Model
C
"RS CVn": T_eff = 5000
log g = 3.0
Sun: T_eff = 5780
log g = 4.44
(isothermal model)
"RS CVn"
10⁻⁵
10⁻⁴
10⁻³
10⁻²
10⁻¹
1
10
m (gm cm⁻²)

Fig. 8

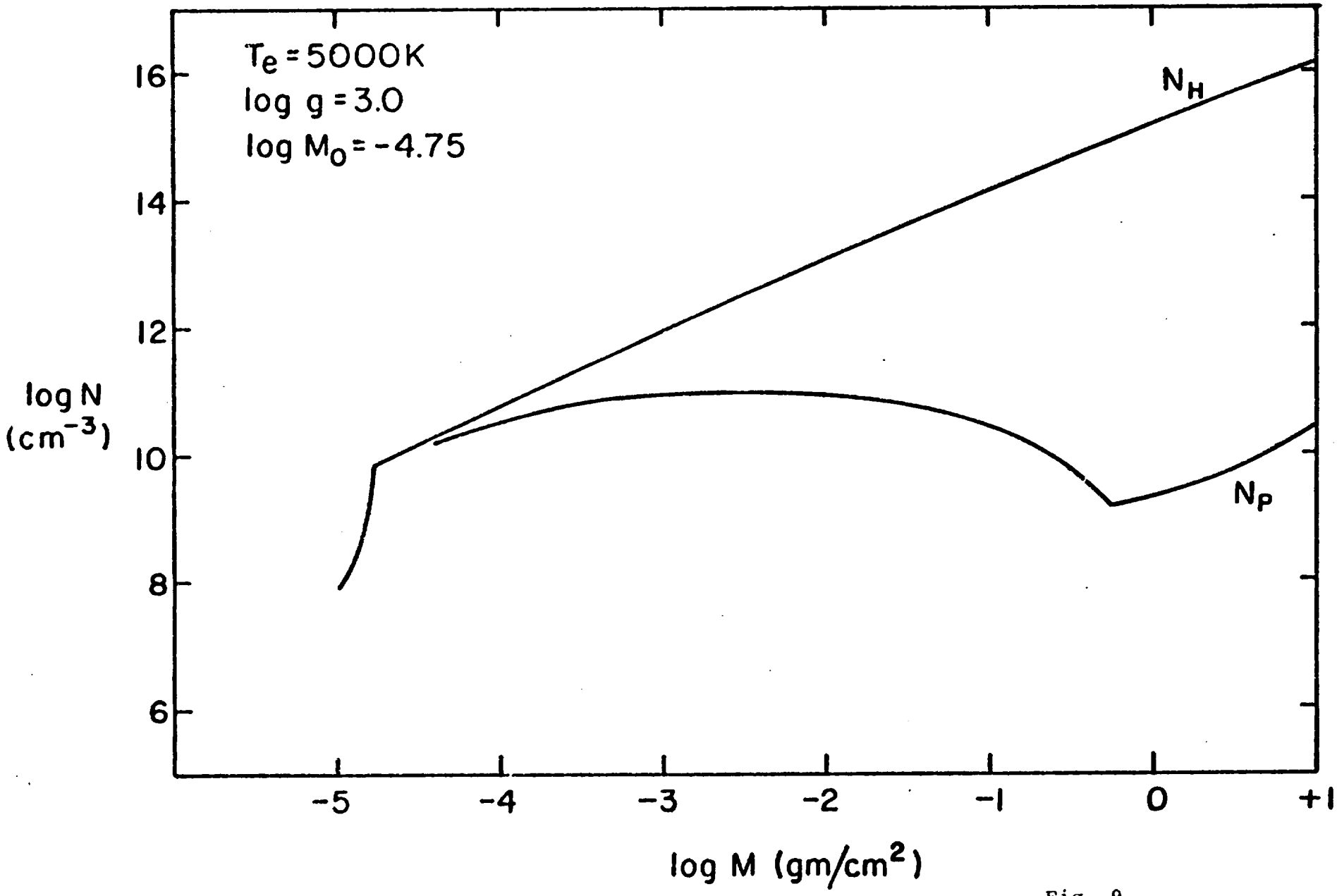
$T_e = 5000K$
log g = 3.0
log M_0 = -4.75
N_H
N_P
16
14
12
10
8
6
log N
(cm^{-3})
-5
-4
-3
-2
-1
0
+1
log M (gm/cm^2)

Fig. 9

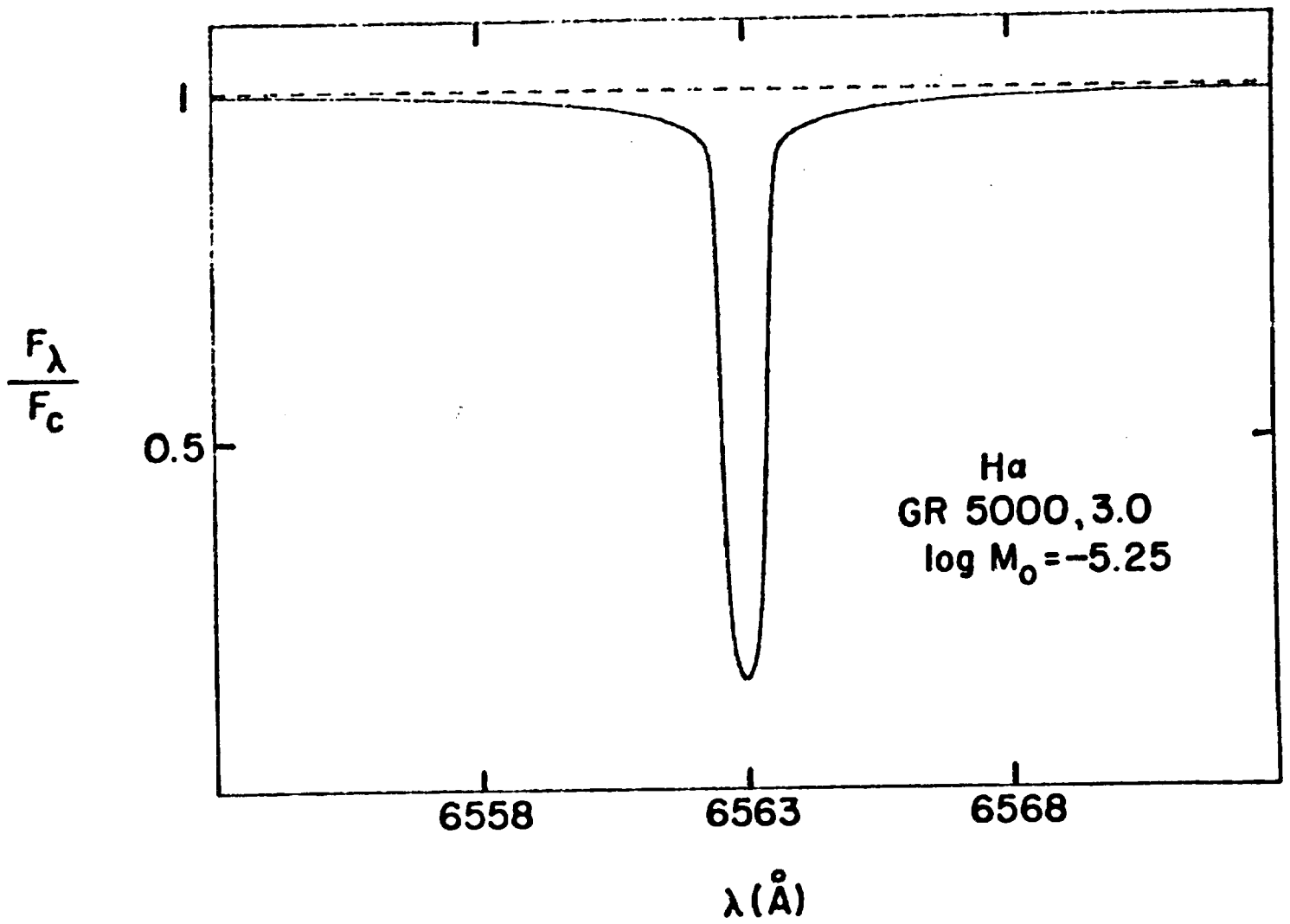

Fig. 1C(a)

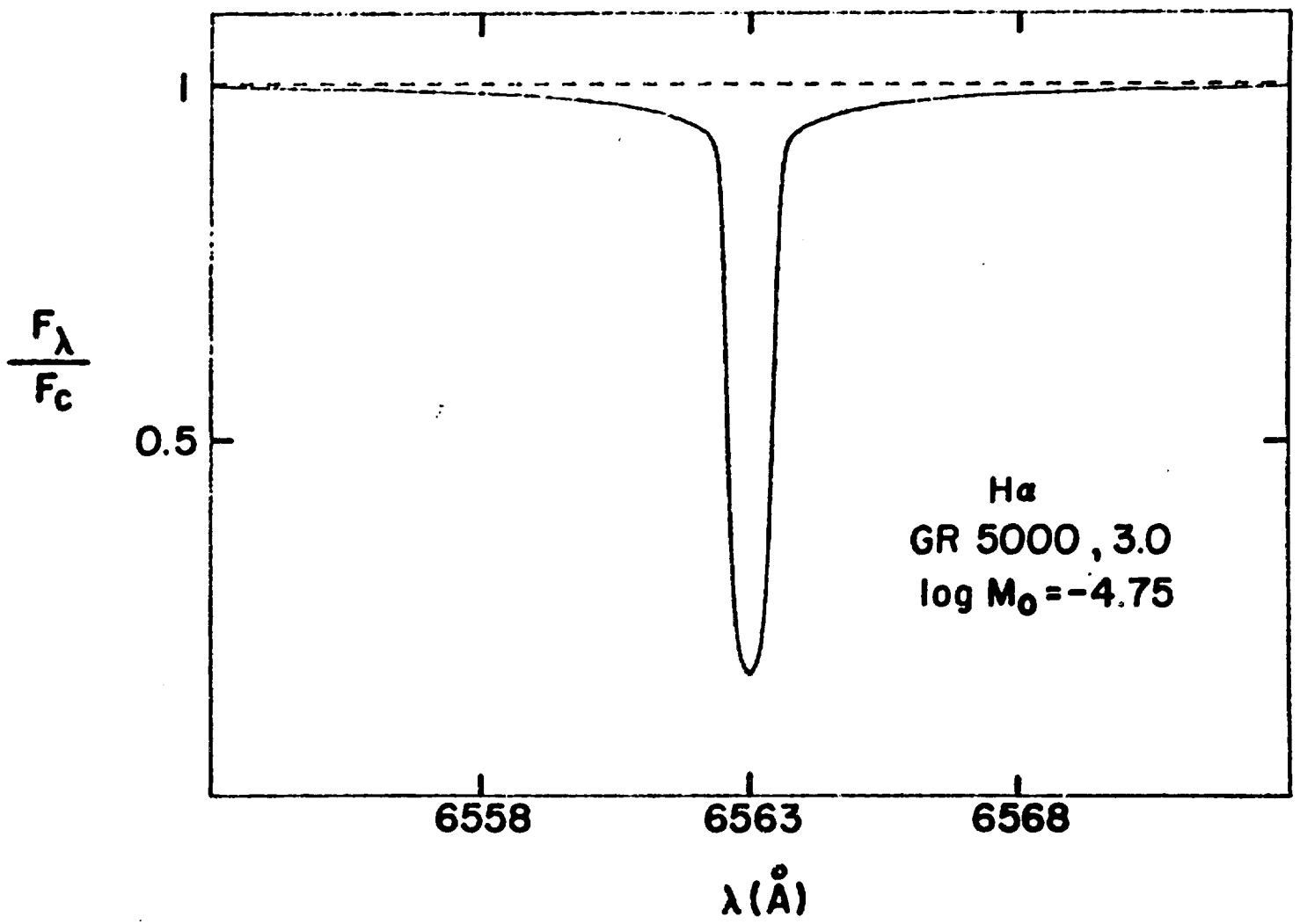

Fig. 10(b)

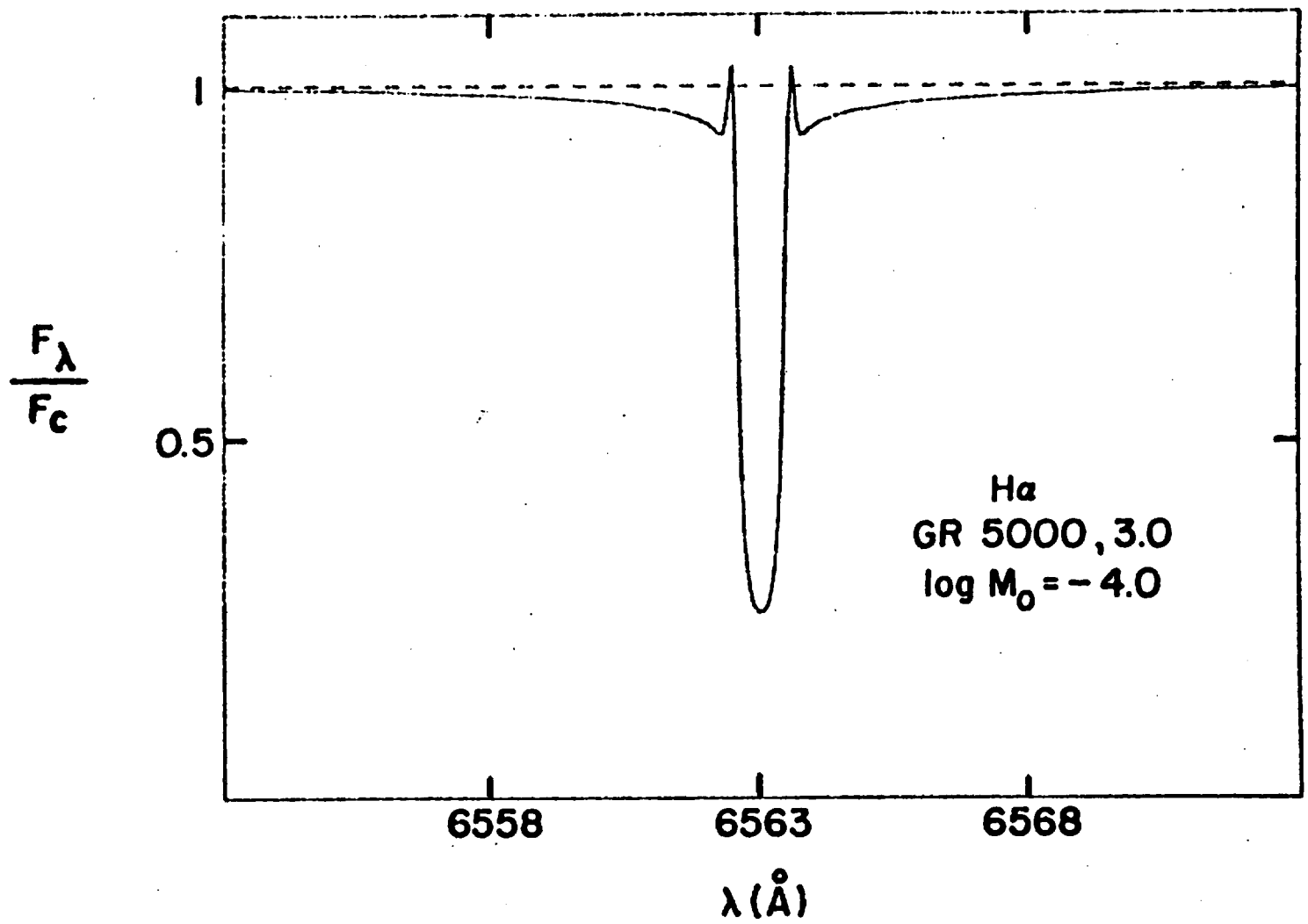

Fig. 10(c)

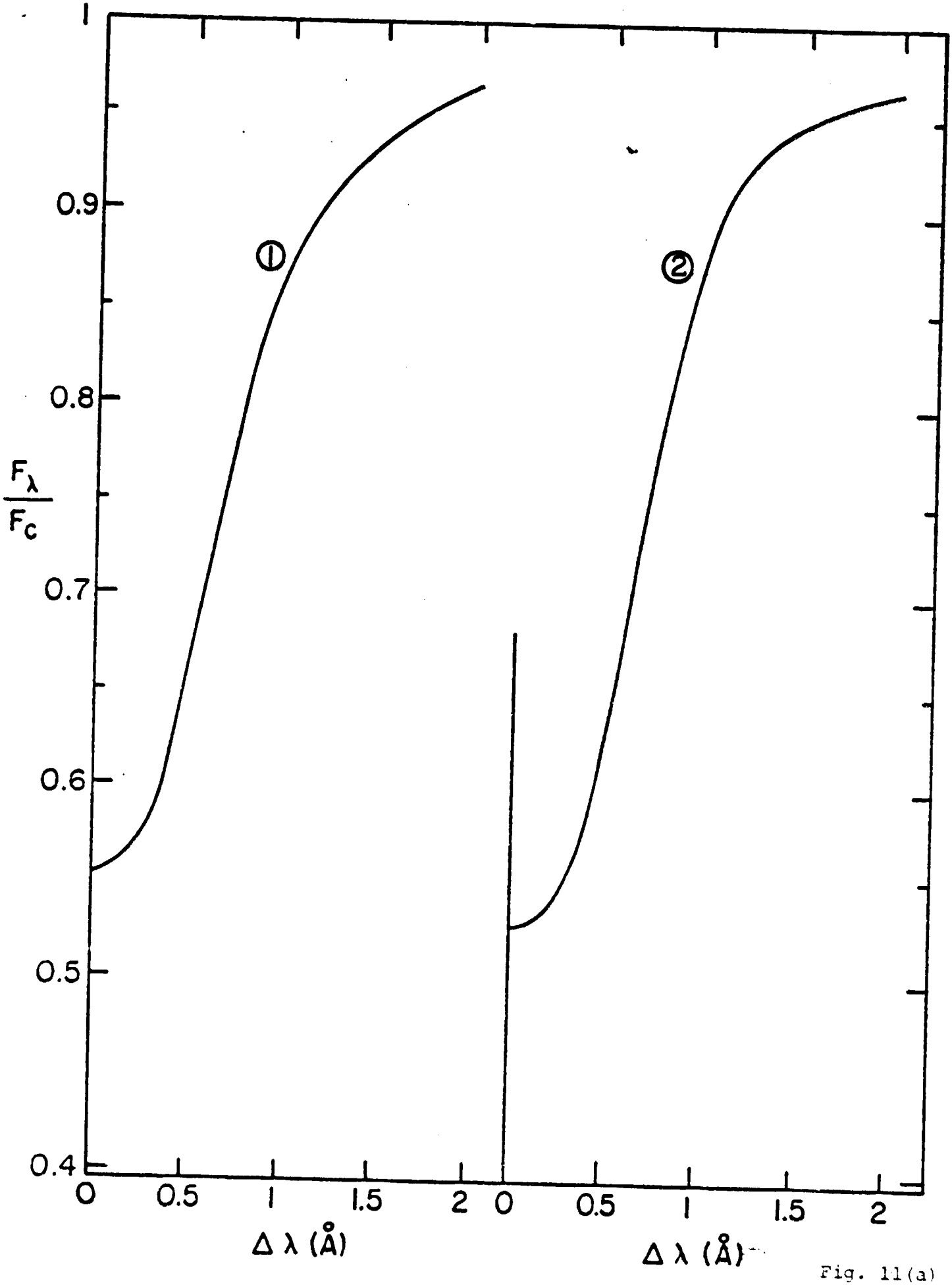

Fig. 11(a)

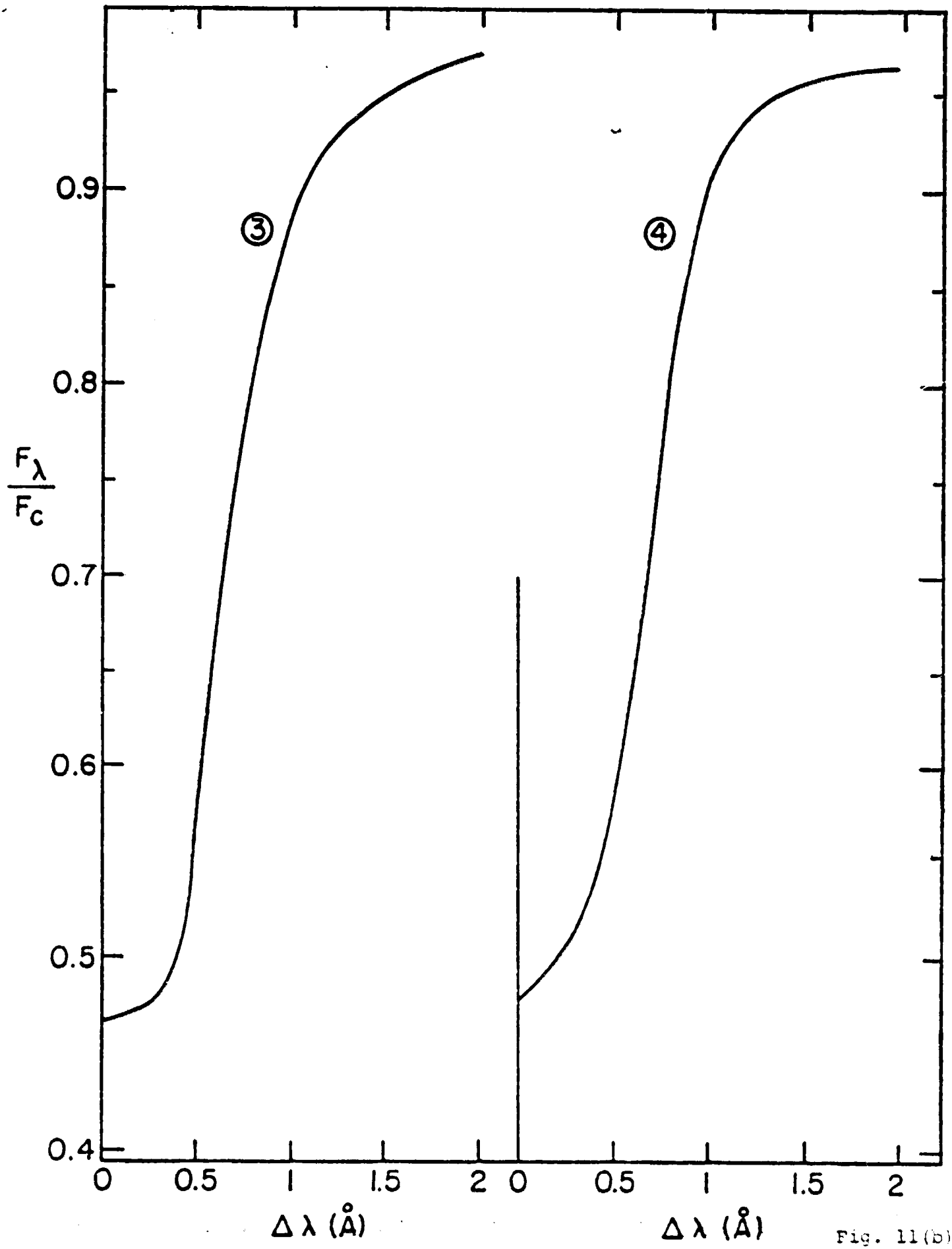

Fig. 11(b)

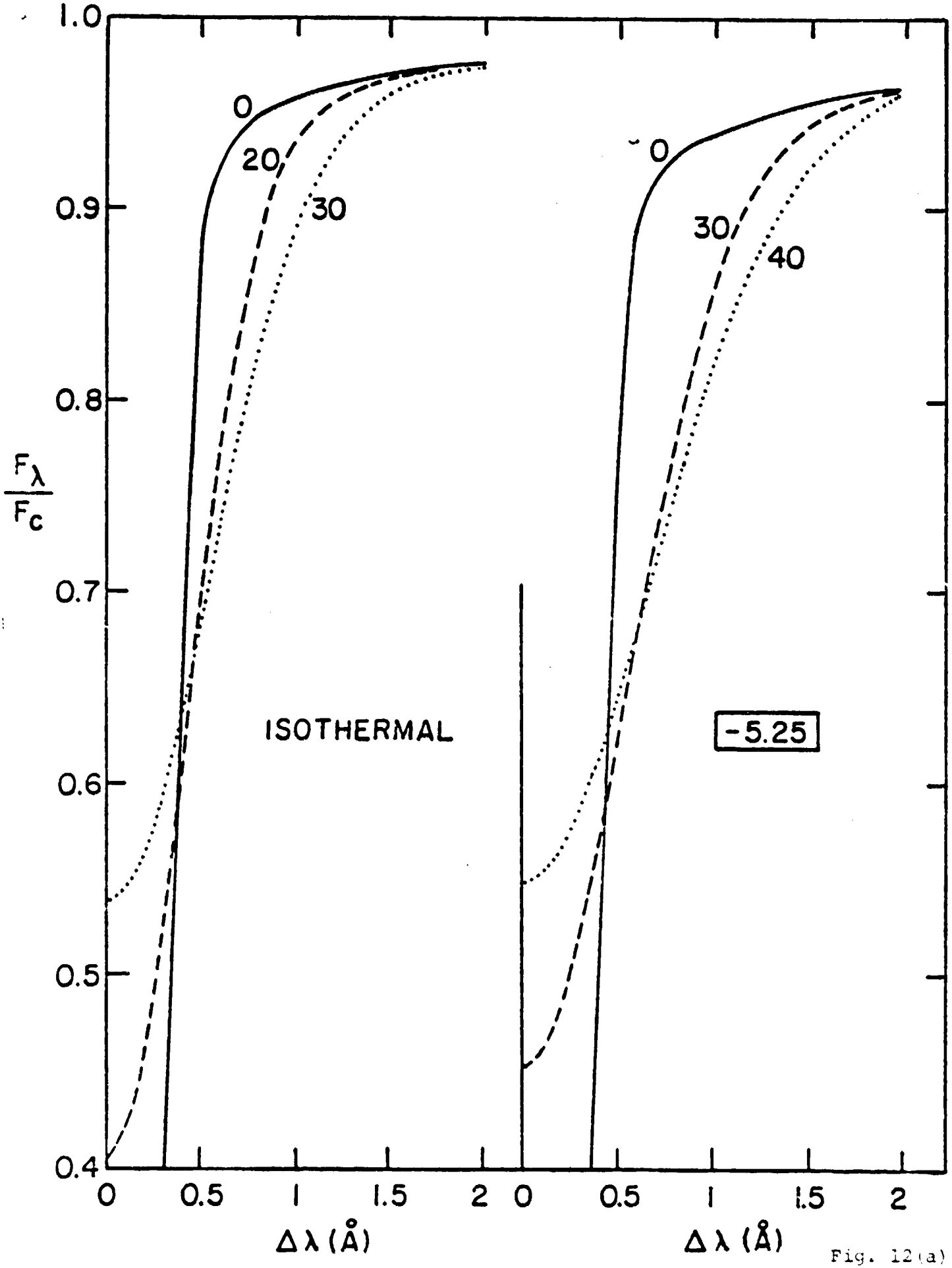
1.0
0.9
0.8
0.7
0.6
0.5
0.4
$\frac{F_\lambda}{F_c}$
0
20
30
0
30
40
ISOTHERMAL
-5.25
0
0.5
1
1.5
2
0
0.5
1
1.5
2
Δλ (Å)
Δλ (Å)

Fig. 12(a)

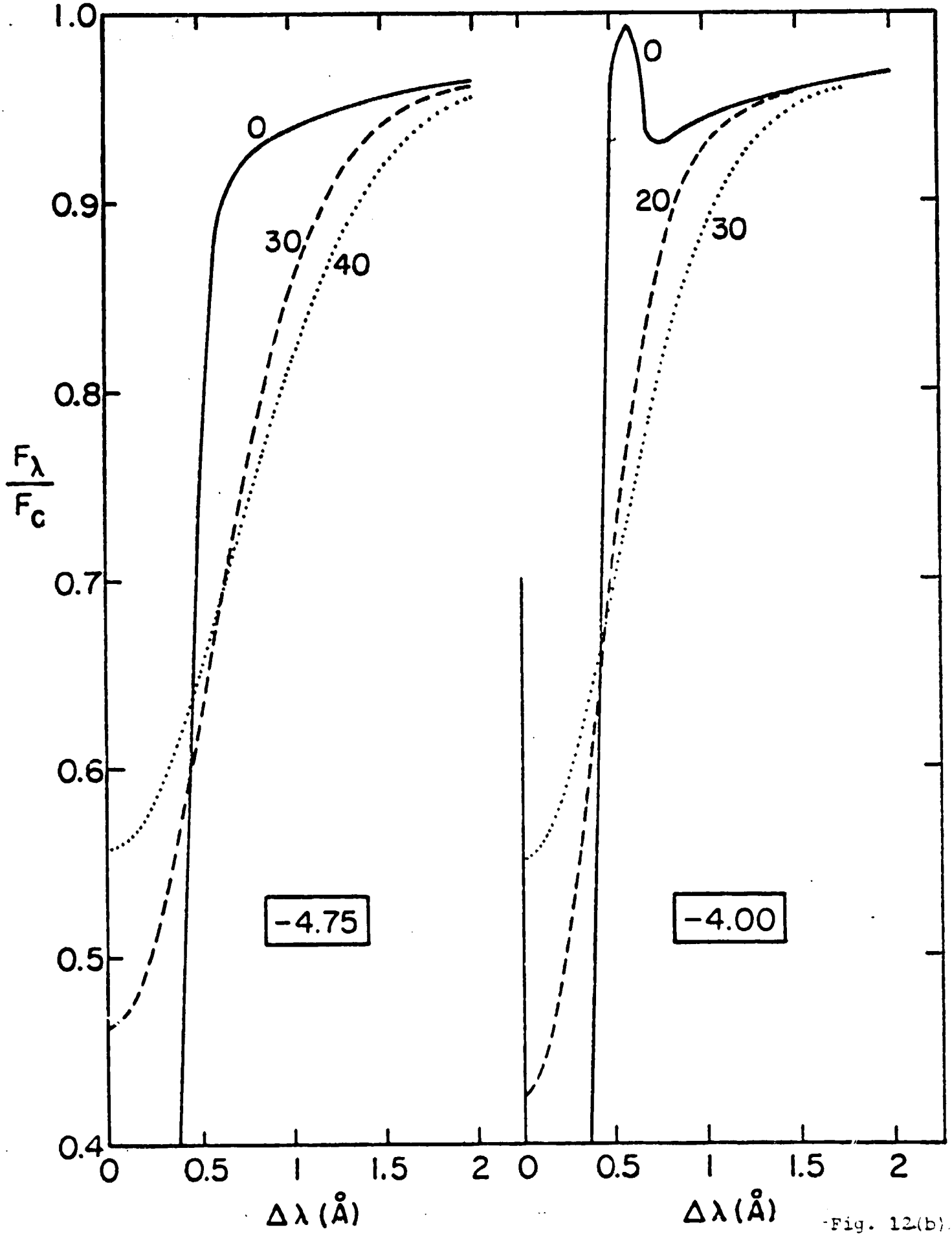
1.0
0.9
0.8
0.7
0.6
0.5
0.4
$\frac{F_\lambda}{F_c}$
0
30
40
-4.75
0
20
30
-4.00
0
0.5
1
1.5
2
$\Delta\lambda$ (Å)

Fig. 12(b)

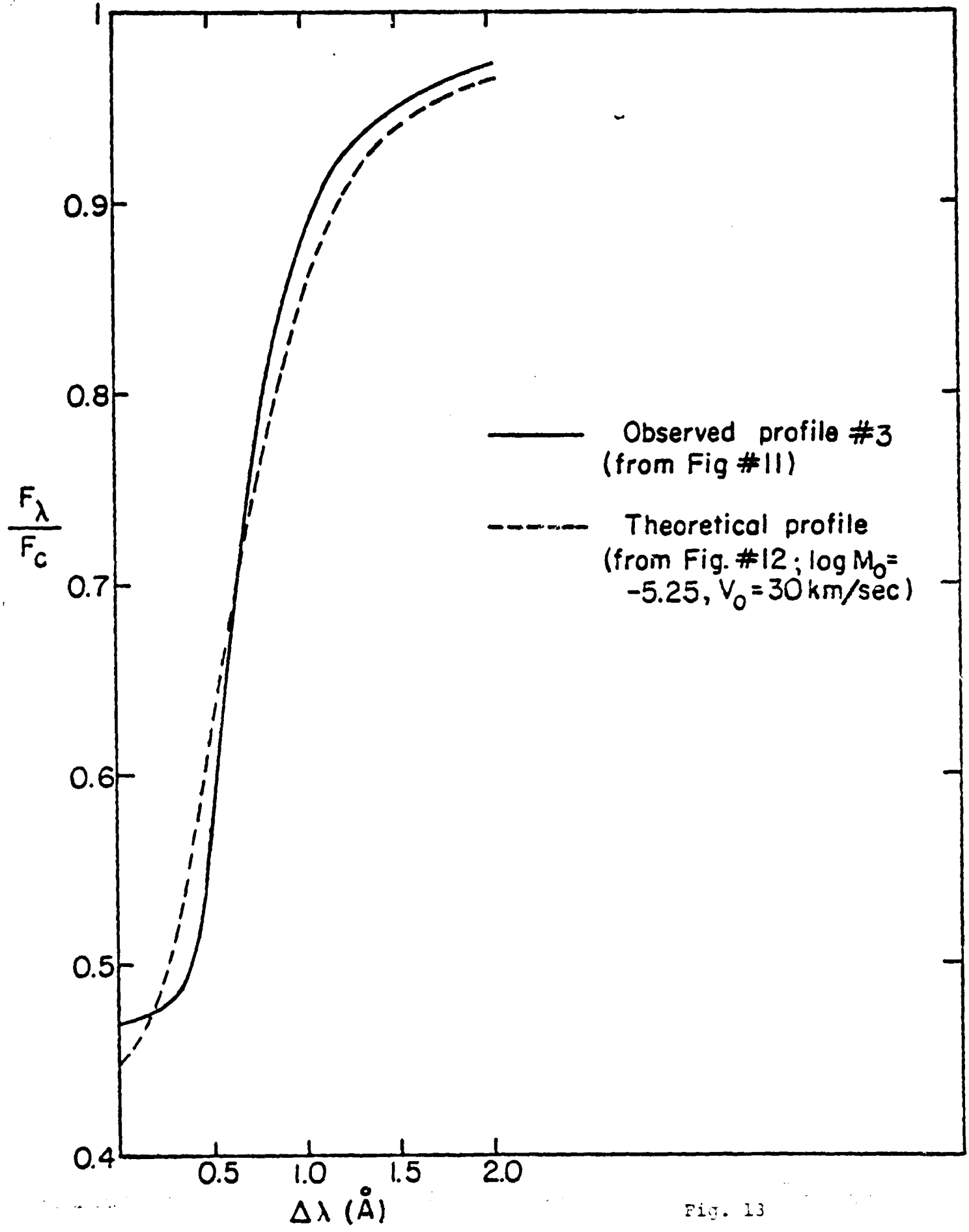
1
0.9
0.8
0.7
0.6
0.5
0.4
$\frac{F_\lambda}{F_c}$
0.5
1.0
1.5
2.0
Δλ (Å)
Observed profile #3
(from Fig #11)
Theoretical profile
(from Fig. #12 ; log M_0=
-5.25, V_0 = 30 km/sec)

Fig. 13